

Towards the HEFT-hedron: the complete set of positivity constraints at NLO

Debsubhra Chakraborty  ^a Susobhan Chattopadhyay  ^a Rick S. Gupta  ^a

^aTata Institute of Fundamental Research, Homi Bhabha Road, Colaba, Mumbai 400005, India

E-mail: debsubhra.chakraborty@tifr.res.in ,

susobhan.chattopadhyay@tifr.res.in, rsgupta@theory.tifr.res.in

ABSTRACT: We present the complete set of positivity bounds on the Higgs Effective Field Theory (HEFT) at next-to-leading order (NLO). We identify the 15 operators that can be constrained by positivity, as they contribute to s^2 -growth in the amplitude for longitudinal gauge-Higgs scattering, that is to all possible 2-to-2 scattering processes involving longitudinal gauge bosons, $V_L = W_L^\pm, Z_L$, and the Higgs boson, h . We find two sets of constraints: (i) specific linear combinations of CP-even Wilson coefficients (WCs) must be positive, and (ii) the magnitudes of some WCs—including all CP-odd ones—must be smaller than products of other CP-even WCs. We present our final constraints on the 15 dimensional HEFT space and show how known positivity bounds on the 3 dimensional space of dimension 8 SMEFT can be recovered from them. We find that only about 5% of the parameter space for WCs of HEFT operators at NLO complies with these positivity constraints. Additionally, we obtain double-sided bounds on these WCs by fully exploiting the implications of unitarity and st -crossing symmetry. For WCs contributing to the vector boson scattering process our final constraints are in most cases significantly stronger than the experimental ones. For the $V_L V_L, hh \rightarrow hh$ and $V_L V_L, hh \rightarrow V_L h$ process, there are no reported experimental limits and our theoretical constraints provide the first bounds.

Contents

1	Introduction	1
2	Parametrizing longitudinal gauge-Higgs scattering	3
2.1	HEFT parametrization	4
2.2	$U(1)_{em}$ parametrization using anomalous couplings	5
2.3	SMEFT parametrization	10
2.4	Longitudinal gauge-Higgs scattering amplitude	13
3	The positivity cone: analytical positivity constraints	15
4	Capping the positivity cone: double sided bounds from s-t crossing and unitarity.	19
5	Visualizing the HEFT-hedron: final positivity constraints	23
5.1	Positivity constraints on HEFT WCs	24
5.2	Positivity constraints in the SMEFT	27
6	Conclusions	30
A	Vector boson scattering in the unitary gauge	32
B	Derivation of Positivity Constraints on HEFT Operators at NLO	32
C	Implications of SMEFT constraints on the $V_L V_L \rightarrow V_L V_L, hh$ process	35

1 Introduction

The discovery of the Higgs boson [1, 2] was a landmark event in the history of particle physics. A detailed characterisation of the Higgs and electroweak sector is arguably the most concrete goal of particle physics research today. In the absence of any direct signs of new physics at the Large Hadron Collider (LHC), effective field theories (EFT) provide a natural framework to parameterise deviations in Higgs and electroweak physics from Standard Model (SM) predictions.

The Standard Model Effective Field Theory (SMEFT)—that extends the Standard Model (SM) lagrangian by a series of higher dimensional operators—has thus become the standard way to parameterise deviations in indirect searches for both experimentalists and theorists. This has led to a sophisticated program of devising experimental strategies to optimally and maximally probe the space of the Wilson coefficients (WCs) of SMEFT operators. An important development, complementing this experimental program, has been

the use of theoretical principles like causality/analyticity, locality, unitarity and crossing symmetry to provide rigorous bounds on this space of EFT coefficients. It was shown in Ref. [3]¹ that the above theoretical principles enforce the positivity of the WCs that give s^{2n} growth in the forward amplitude for $2 \rightarrow 2$ scattering of goldstones and photons, $n \geq 1$ being an integer. A lot of recent work has focused on further extending these arguments to maximally constrain the space of WCs. This has culminated in the derivation of the full set of constraints from $2 \rightarrow 2$ scattering on the space of EFT WCs for causal and unitary theories [7–11]— thus giving rise to the so-called ‘EFT-hedron’ [10], the volume within which the WCs must lie.

In the SMEFT this approach has led to positivity bounds on the coefficient of the s^2 term in the forward amplitude which in turn can be translated to bounds on the WCs of operators at the dimension-8 (D8) level—the lowest order at which an s^2 growth in amplitudes becomes possible [12–17].² It has been recently shown that the more optimal application of unitarity and crossing symmetry developed in Ref. [8, 9], can complement these constraints by providing double sided bounds on WCs [18]. The phenomenological relevance of the SMEFT positivity bounds is, however, somewhat limited because the leading deviations from the SM are parameterised by dimension-6 operators that are not subject to positivity bounds.

As is increasingly being recognised, however, the SMEFT is the not the most general framework to characterise indirect effects. The space of SMEFT WCs at a given order, is in fact a subspace of the more general Higgs EFT (HEFT). This is because of the implicit assumptions made while writing the SMEFT lagrangian. First, unlike the SMEFT, in the HEFT it is not assumed that the observed Higgs boson, h , is part of the electroweak doublet that breaks electroweak symmetry. Furthermore, even in theories where h is part of a electroweak symmetry breaking doublet, if the states being integrated out obtain a large fraction of their mass from the electroweak VEV, the resulting low energy theory is the HEFT and not the SMEFT [19–21].

In this work we obtain the complete set of positivity bounds on HEFT lagrangian at the next to leading order (NLO). The bounds apply to WCs of 15 operators in the NLO lagrangian with 4 derivatives that contribute to scattering of Higgs and longitudinal gauge bosons, i.e. to the $V_L V_L \rightarrow V_L V_L$, hh , $hh \rightarrow V_L h$, hh and $V_L h \rightarrow V_L h$ processes processes, where $V_L = W_L^\pm, Z_L$ are the longitudinal components of the electroweak bosons and h is the observed Higgs boson. No other process has a forward amplitude growing as s^2 or faster in the HEFT NLO lagrangian. First, we consider elastic scattering between superpositions of gauge and Higgs bosons to obtain analytical positivity constraints. These result in an allowed region that forms a convex cone [22] occupying about 5% of the HEFT parameter space. We then use the methods developed in Refs. [8, 9, 18] to numerically derive double-sided bounds to cap this conical region. While ours is the first work to derive positivity constraints for the HEFT, there have been previous works that considered vector boson

¹An earlier application of similar ideas to the chiral lagrangian was made in Ref. [4–6].

²In fact, the positivity bounds, in general, constrain a sum of dimension-8 WCs and a quadratic function of dimension-6 WCs. Nevertheless, it has been possible to individually constrain the dimension-8 contribution [13–15] as we discuss briefly in Sec. 2.3.

scattering to derive some of the positivity constraints on the higgsless electroweak chiral lagrangian [23, 24]. Even for this case, we go beyond the work of Refs. [23, 24]—first, by deriving the complete set of analytical positivity constraints on the WCs involved, and then by imposing double sided bounds on them.

The positivity bounds for HEFT are phenomenologically more relevant compared to the SMEFT case, because they appear already at the next leading order. It is also worth emphasizing that being the most general lagrangian at the weak scale, it is the HEFT, and not the SMEFT, that provides the most general parametrization of the coefficient of the s^2 term in the forward amplitude for longitudinal gauge-Higgs scattering. We show this explicitly in the next section. Existing positivity bounds on SMEFT constrain a set of 3 dimension-8 operators. We will show how these known SMEFT results can be recovered by obtaining the intersection of the three-dimensional SMEFT hyperplane with the NLO HEFT-hedron, the 15-dimensional region allowed by our positivity bounds.

This paper is organized as follows. In Sec. 2, we parameterize longitudinal gauge-Higgs scattering in the SMEFT, HEFT and by imposing only $U(1)_{em}$. In Sec. 3 we analytically derive positivity constraints that result in the aforementioned conical allowed region in the space of HEFT WCs. We then use the methods of Ref. [8, 9, 18] to numerically obtain double-sided bounds to cap this positivity cone in Sec. 4. In Sec. 5 we show our final results and compare them with existing experimental bounds. Finally, we provide concluding remarks in Sec. 6.

Note added: The main results of this work were already presented in the general meeting of the LHC EFT working group on December 2, 2024 [25]. As we were in the final stages of preparing this manuscript, a preprint [26] appeared on the arxiv that has some overlap with our results. Working on the set of 5 custodial invariant HEFT operators at NLO that receive positivity bounds, Ref. [26] derives the analytical positivity bounds mentioned above. Our results in Table 4 are in complete agreement with those of Ref. [26]. Ref. [26] also shows that if the HEFT region allowed by positivity is projected onto the SMEFT plane it contains regions outside the region allowed by positivity in SMEFT. They argue that observation of new physics outside the SMEFT allowed region but within the HEFT allowed region, would indicate that HEFT and not the SMEFT provides the correct low energy description. In Sec. 5.2 we obtain similar results and provide our perspective on how and when positivity can indicate that the low energy theory is not SMEFT but the more general HEFT.

2 Parametrizing longitudinal gauge-Higgs scattering

In this section we present the amplitude for longitudinal gauge-Higgs scattering, i.e. for the $V_L V_L \rightarrow V_L V_L$, $V_L h$, hh , $hh \rightarrow V_L h$, hh and $V_L h \rightarrow V_L h$ processes. We are interested in obtaining the part of the forward amplitude that grows as s^2 and is thus subject to positivity bounds. We will write the amplitude at tree-level using four different parametrizations. For first three parametrizations we will use the following lagrangians: (1) the HEFT NLO lagrangian, (2) a $U(1)_{em}$ parametrization using anomalous couplings and (3) the SMEFT

lagrangian up to the dimension-8 level. Finally, assuming only $U(1)_{em}$ and crossing symmetry, we will provide a general parametrization of the amplitude in terms of Mandelstam invariants and show that there is a one-to-one mapping between the free parameters in this approach and the lagrangian couplings of the first two lagrangian frameworks. In particular we will provide the explicit mapping between these three parametrizations that will make the interpretation of our final bounds on HEFT WCs in terms of anomalous couplings straightforward. The number of parameters in the SMEFT parametrization, however, is smaller than that in the other cases. This implies constraints on the space of HEFT WCs/anomalous couplings if they arise from SMEFT at dimension 8.

2.1 HEFT parametrization

We begin with the HEFT where it is especially straightforward to identify pieces of the gauge Higgs-scattering forward amplitudes that grow as s^2 . In the HEFT lagrangian the observed Higgs boson, h , transforms as a singlet under electroweak symmetry whereas the three goldstone modes associated to the breaking of electroweak symmetry transform non-linearly under it. Here we will follow the formalism in Ref. [27–36] where the spontaneous symmetry breaking pattern is assumed to be,³

$$SU(2)_L \times SU(2)_R \rightarrow SU(2)_C, \quad (2.1)$$

$SU(2)_R$ and $SU(2)_C$ being approximate symmetries. The resulting goldstones, ϕ_I , reside in the matrix, $U = \exp\left\{\left[\frac{i}{v}\phi_I\sigma^I\right]\right\}$, where, $I \in 1, 2, 3$ and $v = 246$ GeV is the electroweak VEV. The transformation of U under the group $SU(2)_L \otimes SU(2)_R$ is given by,

$$U(x) \rightarrow LU(x)R^\dagger. \quad (2.2)$$

and the covariant derivative of U is defined as, $D_\mu U = \partial_\mu U + i\hat{W}_\mu U - iU\hat{B}_\mu$ where,

$$\hat{W}_\mu = g\frac{\vec{\sigma}}{2}\vec{W}_\mu; \quad \hat{B}_\mu = g'\frac{\sigma_3}{2}B_\mu. \quad (2.3)$$

The building blocks of the HEFT lagrangian are,

$$\mathbf{V}_\mu = iUD_\mu U^\dagger \quad \mathbf{T} = U\frac{\sigma_3}{2}U^\dagger \quad (2.4)$$

and the observed Higgs h , which transform as follows,

$$\mathbf{V}_\mu \rightarrow L\mathbf{V}_\mu L^\dagger \quad \mathbf{T} \rightarrow L\mathbf{T}L^\dagger \quad h \rightarrow h. \quad (2.5)$$

The presence of a σ_3 in the definition of \mathbf{V}_μ and \mathbf{T} explicitly breaks $SU(2)_R \rightarrow U_Y(1)$ in the HEFT lagrangian (see for eg. the discussion in Ref. [38]).

The list of NLO operators in the HEFT, presented in different works (see Ref. [32–36]) differ from each other based on the criteria used by the authors in organising the HEFT expansion. In all these lists, however, the only operators, that can result in an s^2 growth in

³See Ref. [37, 38] for an alternative formulation with the spontaneous symmetry breaking pattern, $SU(2)_L \times U(1)_Y \rightarrow U(1)_{em}$.

a $2 \rightarrow 2$ scattering process are those with 4 derivatives and no field strengths, i.e. operators of the form of the UhD^4 . Note that $2 \rightarrow 2$ scattering amplitudes involving fermions and photons do not receive NLO HEFT contributions that grow faster than s^2 . Thus in order to obtain the complete set of positivity bounds on the HEFT at NLO, it suffices to consider only longitudinal gauge-Higgs scattering.

In Table 1, we reproduce the list of all the 15 operators of type UhD^4 presented in Ref. [36]. These operators contribute to the amplitude for Higgs and goldstone scattering, $\phi_i \phi_j \rightarrow \phi_k \phi_l$ with the indices taking values from 1–4 and $\phi_4 \equiv h$; this amplitude is identical to longitudinal gauge-Higgs scattering in the high energy limit by the goldstone boson equivalence theorem [39]. The functions, $\mathcal{F}_i^{UhD^4}(h)$, in Table (1) are given by,

$$\mathcal{F}_i^{UhD^4}(h) = 1 + \sum_{r=1} c_{ir}^{UhD^4} \left(\frac{h}{v} \right)^r$$

for $i = 1, \dots, 15$. These operators appear in the NLO HEFT lagrangian at NLO as follows,

$$\mathcal{L}_{HEFT}^{NLO} \supset \sum_{n=1}^{15} c_i \mathcal{O}_i^{UhD^4} + \dots \quad (2.6)$$

where c_i is the WC of the operator, $\mathcal{O}_i^{UhD^4}$. As far as the power-counting for these WCs is concerned, we assume,

$$c_i \sim v^2 \Lambda^2 \left(\frac{D}{\Lambda} \right)^{n_D} \left(\frac{h}{v} \right)^{n_h} \quad (2.7)$$

where $v/\Lambda \geq 1/4\pi$. As we will soon discuss, if these HEFT operators arise from SMEFT, the fact that $SU(2)_L \times U(1)_Y$ is then linearly realised, will imply further suppression in some linear combinations of the WCs.

Note that while presenting the longitudinal gauge-Higgs scattering amplitudes, we will consider only a single insertion of a HEFT NLO WC. If we consider more insertions, operators from other categories in Ref. [36], for eg. $UhD^2 X$, might also result in s^2 growth in the amplitude. These contributions will, however, be suppressed given the power counting scheme in eq. (2.7) and can therefore be safely ignored.

2.2 $U(1)_{em}$ parametrization using anomalous couplings

We now present a $U(1)_{em}$ invariant lagrangian containing all possible vertices to parametrize longitudinal gauge-higgs scattering. The couplings accompanying individual $U(1)_{em}$ invariant lagrangian terms are called anomalous couplings. These anomalous couplings provide an especially convenient parametrization of deviations beyond the SM in experimental and phenomenological studies.

To obtain an amplitude that grows as s^2 , the anomalous vertices can be of the following forms: $\partial V V^2, V^4, \partial h V^3, (\partial h)^2 V^2, (\partial h)^3 V$ and $(\partial h)^4$. While the $\partial V V^2$ terms contribute via tree-level exchange diagrams, the rest of the vertices are contact terms. That these terms can lead to an s^2 growth can be understood by recalling that longitudinally polarised vector bosons, $V_L^\mu = W_L^{\pm, \mu}, Z_L^\mu$, contribute a longitudinal polarization

Process	i	$\mathcal{O}_i^{Uhd^4}$	CP	$SU(2)_C$
$V_L V_L \rightarrow V_L V_L$	1	$\langle \mathbf{V}_\mu \mathbf{V}^\mu \rangle^2 \mathcal{F}_1^{Uhd^4}(h)$	+	P
	2	$\langle \mathbf{V}_\mu \mathbf{V}_\nu \rangle \langle \mathbf{V}^\mu \mathbf{V}^\nu \rangle \mathcal{F}_2^{Uhd^4}(h)$	+	P
	3	$\langle \mathbf{T} \mathbf{V}_\mu \rangle \langle \mathbf{T} \mathbf{V}_\nu \rangle \langle \mathbf{V}^\mu \mathbf{V}^\nu \rangle \mathcal{F}_3^{Uhd^4}(h)$	+	V
	4	$\langle \mathbf{T} \mathbf{V}_\mu \rangle \langle \mathbf{T} \mathbf{V}^\mu \rangle \langle \mathbf{V}^\nu \mathbf{V}_\nu \rangle \mathcal{F}_4^{Uhd^4}(h)$	+	V
	5	$(\langle \mathbf{T} \mathbf{V}_\mu \rangle \langle \mathbf{T} \mathbf{V}^\mu \rangle)^2 \mathcal{F}_5^{Uhd^4}(h)$	+	V
$V_L V_L \rightarrow V_L h$	6	$\langle \mathbf{V}_\mu \mathbf{V}^\mu \rangle \langle \mathbf{T} \mathbf{V}_\nu \rangle \frac{D^\nu h}{v} \mathcal{F}_6^{Uhd^4}(h)$	-	V
	7	$\langle \mathbf{V}_\mu \mathbf{V}_\nu \rangle \langle \mathbf{T} \mathbf{V}^\mu \rangle \frac{D^\nu h}{v} \mathcal{F}_7^{Uhd^4}(h)$	-	V
	8	$i \langle \mathbf{T} \mathbf{V}_\mu \mathbf{V}_\nu \rangle \langle \mathbf{T} \mathbf{V}^\mu \rangle \frac{D^\nu h}{v} \mathcal{F}_8^{Uhd^4}(h)$	+	V
	9	$\langle \mathbf{T} \mathbf{V}_\mu \rangle \langle \mathbf{T} \mathbf{V}^\mu \rangle \langle \mathbf{T} \mathbf{V}_\nu \rangle \frac{D^\nu h}{v} \mathcal{F}_9^{Uhd^4}(h)$	-	V
$V_L V_L \rightarrow hh$	10	$\langle \mathbf{V}_\mu \mathbf{V}_\nu \rangle \frac{h D^\mu D^\nu h}{v^2} \mathcal{F}_{10}^{Uhd^4}(h)$	+	P
	11	$\langle \mathbf{V}_\mu \mathbf{V}^\mu \rangle \frac{D_\nu h D^\nu h}{v^2} \mathcal{F}_{11}^{Uhd^4}(h)$	+	P
	12	$\langle \mathbf{T} \mathbf{V}_\mu \rangle \langle \mathbf{T} \mathbf{V}_\nu \rangle \frac{h D^\mu D^\nu h}{v^2} \mathcal{F}_{12}^{Uhd^4}(h)$	+	V
	13	$\langle \mathbf{T} \mathbf{V}_\mu \rangle \langle \mathbf{T} \mathbf{V}^\mu \rangle \frac{D_\nu h D^\nu h}{v^2} \mathcal{F}_{13}^{Uhd^4}(h)$	+	V
$V_L h \rightarrow hh$	14	$\langle \mathbf{T} \mathbf{V}_\mu \rangle \frac{h D^\nu h D_\nu D^\mu h}{v^3} \mathcal{F}_{14}^{Uhd^4}(h)$	-	V
$hh \rightarrow hh$	15	$\frac{1}{v^4} h^2 (D_\mu D_\nu h) (D^\mu D^\nu h) \mathcal{F}_{15}^{Uhd^4}(h)$	+	P

Table 1: The list of 15 operators of type Uhd^4 in the HEFT lagrangian at NLO in the basis of Ref. [36]. These are the complete set of operators at NLO that contribute to the s^2 piece in the forward amplitude for $2 \rightarrow 2$ scattering involving goldstones and the Higgs boson—and thus to the s^2 piece in the forward amplitude of longitudinal gauge-Higgs scattering. We also provide the CP properties of the operators in the fourth column, while the fifth column indicates whether each operator preserves (P) or violates (V) the custodial symmetry, $SU(2)_C$. The contractions of $SU(2)$ group indices between \mathbf{T} and \mathbf{V}_μ are represented by the symbol $\langle \dots \rangle$.

vector, $\epsilon_{L,\mu}^V \approx p_\mu/m_V$, to the amplitude. We modify the SM lagrangian by adding terms of each of the above categories,

$$\mathcal{L}_{BSM} \supset \mathcal{L}_{SM} + \Delta \mathcal{L}_{\partial V V^2} + \Delta \mathcal{L}_{V^4} + \mathcal{L}_{(\partial h)^2 V^2} + \mathcal{L}_{\partial h V^3} + \mathcal{L}_{(\partial h)^3 V} + \mathcal{L}_{(\partial h)^4}. \quad (2.8)$$

As already mentioned in the previous section we ignore contributions to the amplitude involving two insertions of BSM couplings.

Let us begin with vertices of the form $\partial V V^2$ formed out of 3 gauge bosons and a single derivative, the so-called Triple Gauge couplings (TGC), that were first presented in

Ref. [40],

$$\begin{aligned}\Delta\mathcal{L}_{\partial VV^2} = & igc_{\theta_W} [\delta g_1^Z Z_\mu (W_\nu^- \mathcal{W}^{+\mu\nu} - W_\nu^+ \mathcal{W}^{-\mu\nu}) + \delta\kappa^Z W_\mu^- W_\nu^+ Z^{\mu\nu}] \\ & + ie \delta\kappa^\gamma W_\mu^- W_\nu^+ A^{\mu\nu} - g_4 W_\mu^- W_\nu^+ (\partial^\mu V^\nu + \partial^\nu V^\mu) + g_5 \epsilon^{\mu\nu\rho\sigma} W_\mu^+ \overleftrightarrow{D}_\rho W_\nu^- Z_\sigma \\ & + igc_{\theta_W} \delta\tilde{\kappa}^Z W_\mu^- W_\nu^+ \tilde{Z}^{\mu\nu} + ie \delta\tilde{\kappa}^\gamma W_\mu^- W_\nu^+ \tilde{A}^{\mu\nu}.\end{aligned}\quad (2.9)$$

where,

$$\mathcal{W}^{+\mu\nu} = D_\mu^e W^{+,\nu} - D_\nu^e W^{+,\mu}, \quad (2.10)$$

$D_\mu^e = \partial_\mu + ieA_\mu$ being the covariant derivative. In the above lagrangian the first three terms are even under both charge conjugation (C) and parity (P), while all other terms are either C-odd or P-odd or both. As far as longitudinal vector boson scattering is concerned, single insertions of only P and CP-even vertices can lead to an s^2 growth in the amplitude.

The HEFT contributions to the three C and P-even TGCs do not arise from the operators in Table 1, but from the following three other operators from the NLO basis of Ref. [36],

$$\beta_0 \frac{v^2}{2} \langle \mathbf{TV}_\mu \rangle \langle \mathbf{TV}^\mu \rangle + \alpha_{33} g^2 \langle \mathbf{TW}_{\mu\nu} \rangle \langle \mathbf{TW}^{\mu\nu} \rangle + \alpha_{WB} \frac{gg'}{2} \langle \mathbf{TW}_{\mu\nu} \rangle B^{\mu\nu} \quad (2.11)$$

where $\mathbf{W}_{\mu\nu} = W_{\mu\nu}^a \sigma^a / 2$. Working in the input parameter scheme, $\{m_W, m_Z, \alpha_{em}\}$, we evaluate the contributions from the operators in eq. (2.11) to the above anomalous couplings in the unitary gauge, carefully taking into account input parameter redefinitions. This gives,

$$\begin{aligned}\delta g_Z^1 &= \frac{1}{2s_{\theta_W}^2} \frac{\delta m_Z^2}{m_Z^2}, \quad \delta\kappa^\gamma = -\frac{g^2}{2} \alpha_{WB} - g^2 \alpha_{33} \\ \delta\kappa^Z &= \frac{1}{2s_{\theta_W}^2} \frac{\delta m_Z^2}{m_Z^2} + \frac{g^2}{2} t_{\theta_W}^2 \alpha_{WB} - g^2 \alpha_{33},\end{aligned}\quad (2.12)$$

where,

$$\frac{\delta m_Z^2}{m_Z^2} = \beta_0 - g^2 t_{\theta_W}^2 \alpha_{WB} + g^2 \alpha_{33} \quad (2.13)$$

We will show in Appendix A that once the V^4 vertices arising from the operators in eq. (2.11) are also taken into account, their contribution to the s^2 piece in the $V_L V_L \rightarrow V_L V_L$ amplitude exactly cancels the TGC contributions in eq. (2.12). Thus, the operators in eq. (2.11) ultimately do not give s^2 growth in vector boson scattering a fact that can also be understood directly using the goldstone boson equivalence principle. This is, of course, why we do not include these three operators in our list in Table 1.

Vertices of the form V^4 formed of 4 gauge bosons and no derivatives, are called anomalous quartic gauge couplings (aQGC). The following list of all possible $U(1)_{em}$ terms of

this form was presented in Ref. [41],

$$\begin{aligned}\Delta\mathcal{L}_{QGC} &= g^2 c_{\theta_w}^2 \left[\delta g_{ZZ1}^Q Z^\mu Z^\nu W_\mu^- W_\nu^+ - \delta g_{ZZ2}^Q Z^\mu Z_\mu W^{-\nu} W_\nu^+ \right] \\ &+ \frac{g^2}{2} \left[\delta g_{WW1}^Q W^{-\mu} W^{+\nu} W_\mu^- W_\nu^+ - \delta g_{WW2}^Q (W^{-\mu} W_\mu^+)^2 \right] + \frac{g^2}{4c_{\theta_w}^4} h_{ZZ}^Q (Z^\mu Z_\mu)^2\end{aligned}\quad (2.14)$$

We get the following contributions to these from HEFT operators:

$$\begin{aligned}\delta g_{ZZ1}^Q &= \frac{1}{s_{\theta_w}^2} \frac{\delta m_Z^2}{m_Z^2} + \frac{g^2}{4c_{\theta_w}^4} (4c_2 + c_3), & \delta g_{ZZ2}^Q &= \frac{1}{s_{\theta_w}^2} \frac{\delta m_Z^2}{m_Z^2} - \frac{g^2}{4c_{\theta_w}^4} (4c_1 + c_4), \\ \delta g_{WW1}^Q &= \frac{c_{\theta_w}^2}{s_{\theta_w}^2} \frac{\delta m_Z^2}{m_Z^2} + g^2 c_2 - 2g^2 \alpha_{33}, & \delta g_{WW2}^Q &= \frac{c_{\theta_w}^2}{s_{\theta_w}^2} \frac{\delta m_Z^2}{m_Z^2} - g^2 (2c_1 + c_2) - 2g^2 \alpha_{33} \\ h_{ZZ}^Q &= g^2 (4c_1 + 4c_2 + 2c_3 + 2c_4 + c_5) / 4.\end{aligned}\quad (2.15)$$

It might seem confusing at first that while there are only 5 operators contributing to the s^2 piece in the $V_L V_L \rightarrow V_L V_L$ forward amplitudes in the HEFT parametrization, there are 8 anomalous couplings that can give such an effect in the $U(1)_{em}$ invariant parametrization. This, however, does not imply an inconsistency between the two parametrization because only five linear combinations of the 8 anomalous couplings give rise to s^2 growth in the forward amplitude. These five linear combinations can be obtained by inverting eq. (2.12) and eq. (2.15) to write the HEFT WCs, $c_1 - c_5$, in terms of the above TGCs and aQGCs; this is shown in Table 2. This inversion also gives us, β_0, α_{WB} and α_{33} as a linear combination of anomalous couplings,

$$\begin{aligned}\beta_0 &= -c_{\theta_w}^2 \delta g_Z^1 + (1 + s_{\theta_w}^2) \delta \kappa^Z - s_{\theta_w}^2 \delta \kappa^\gamma \\ \alpha_{WB} &= -\frac{2c_{\theta_w}^2}{g^2} (\delta g_Z^1 - \delta \kappa^Z + \delta \kappa^\gamma) \\ \alpha_{33} &= \frac{1}{g^2} (c_{\theta_w}^2 \delta g_Z^1 - c_{\theta_w}^2 \delta \kappa^Z - s_{\theta_w}^2 \delta \kappa^\gamma).\end{aligned}\quad (2.16)$$

The right hand sides in eq. (2.16) above are precisely the linear combinations of anomalous couplings that do not give an s^2 growth in the forward amplitude.

Next we present the the most general non-redundant list of vertices of the form, $(\partial h)^2 V^2$,

$$\begin{aligned}\Delta\mathcal{L}_{(\partial h)^2 V^2} &= \kappa_{WW}^{hh} \frac{h^2}{2v^2} \mathcal{W}^{+\mu\nu} \mathcal{W}_{\mu\nu}^- + \kappa_{ZZ}^{hh} \frac{h^2}{4v^2} Z^{\mu\nu} Z_{\mu\nu} \\ &+ \tilde{\kappa}_{WW}^{hh} \frac{h^2}{2v^2} \mathcal{W}^{+\mu\nu} \tilde{\mathcal{W}}_{\mu\nu}^- + \tilde{\kappa}_{ZZ}^{hh} \frac{h^2}{4v^2} Z^{\mu\nu} \tilde{Z}_{\mu\nu} \\ &+ g_{Z1}^{hh} \frac{g^2}{c_{\theta_w}^2} \frac{(\partial_\nu h)^2 Z_\mu Z^\mu}{v^2} + g_{Z2}^{hh} \frac{g^2}{c_{\theta_w}^2} \frac{\partial_\mu h \partial_\nu h}{2v^2} Z^\mu Z^\nu + g_{W1}^{hh} g^2 \frac{(\partial_\nu h)^2}{v^2} W^{+\mu} W_\mu^- \\ &+ g_{W2}^{hh} g^2 \frac{\partial_\mu h \partial_\nu h}{2v^2} (W^{+\mu} W^{-\nu} + h.c.)\end{aligned}\quad (2.17)$$

All other anomalous couplings can be reduced to the above non-redundant set using field-redefinitions and integration by parts. The anomalous couplings for the contact terms involving field strengths, i.e. κ_{WW}^{hh} and κ_{ZZ}^{hh} , do not contribute to s^2 piece of the forward amplitude.⁴ The other couplings get contributions only from the HEFT operators of Table 1 in the unitary gauge,

$$\begin{aligned} g_{Z1}^{hh} &= \frac{1}{4}(c_{10} + 2c_{11} + c_{12}/2 + c_{13}), & g_{Z2}^{hh} &= -\frac{1}{2}(2c_{10} + c_{12}), \\ g_{W1}^{hh} &= \left(c_{11} + \frac{c_{10}}{2}\right), & g_{W2}^{hh} &= -c_{10}, \end{aligned} \quad (2.18)$$

which clearly establishes a one to one mapping between these anomalous couplings and the HEFT WCs.

As far as couplings of the category $(\partial h)^3 V$ are concerned, the most general lagrangian is,

$$\begin{aligned} \Delta \mathcal{L}^{hV^3} &= igc_{\theta_W} \frac{h}{v} \left[g_{Z1}^{hV^3} Z_\mu (W_\nu^+ \mathcal{W}^{-\mu\nu} - W_\nu^- \mathcal{W}^{+\mu\nu}) + \kappa_Z^{hV^3} W_\mu^+ W_\nu^- Z^{\mu\nu} \right] \\ &+ igc_{\theta_W} \frac{h}{v} \left[\tilde{\kappa}_Z^{hV^3} W_\mu^+ W_\nu^- \tilde{Z}^{\mu\nu} + \tilde{g}_{Z1}^{hV^3} Z_\mu W_\nu^+ \tilde{W}^{-\mu\nu} \right] \\ &+ \frac{h}{v} \left[g_4^{hV^3} Z^\mu (W^{+\nu} W_{\mu\nu}^- + h.c.) + g_5^{hV^3} \epsilon^{\mu\nu\rho\sigma} W_\mu^+ \overleftrightarrow{D}_\rho W_\nu^- Z_\sigma \right] \\ &+ ig_{W1}^{\partial hV^3} \frac{g^3}{2c_{\theta_W}} \frac{\partial^\mu h}{v} Z_\nu (W_\mu^+ W^{-\nu} - h.c.) + g_{W2}^{\partial hV^3} \frac{g^3}{2c_{\theta_W}} \frac{\partial^\mu h}{v} Z_\nu (W_\mu^+ W^{-\nu} + h.c.) \\ &+ g_{W3}^{\partial hV^3} \frac{g^3}{2c_{\theta_W}} \frac{\partial^\mu h}{v} Z_\mu W_\mu^+ W^{-\mu} + g_Z^{\partial hV^3} \frac{g^3}{2c_{\theta_W}^3} \frac{\partial^\mu h}{v} Z_\mu Z_\nu Z^\nu \end{aligned} \quad (2.19)$$

where we have again removed all possible redundancies. Only the anomalous couplings $g_{W1}^{\partial hV^3}$, $g_{W2}^{\partial hV^3}$, $g_{W3}^{\partial hV^3}$ and $g_Z^{\partial hV^3}$ contribute to the s^2 piece of the forward amplitude. Once again we obtain a one to one mapping between these anomalous couplings and four of the HEFT operators of Table 1,

$$g_{W1}^{\partial hV^3} = \frac{c_8}{4}, \quad g_{W2}^{\partial hV^3} = \frac{c_7}{2}, \quad g_{W3}^{\partial hV^3} = c_6, \quad g_Z^{\partial hV^3} = \frac{2c_6 + 2c_7 + c_9}{4}. \quad (2.20)$$

Finally there is one $U(1)_{em}$ invariant operator each in the $\partial h^3 V$ and ∂h^4 categories,

$$\mathcal{L}^{h^3 V} = g^{\partial h^3 V} \frac{g}{2c_{\theta_W} v^3} \partial_\nu h \partial^\nu h \partial_\mu h Z^\mu, \quad \mathcal{L}^{(\partial h)^4} = \frac{g^{(\partial h)^4}}{v^4} \partial_\mu h \partial^\mu h \partial_\nu h \partial^\nu h \quad (2.21)$$

which respectively get contributions from c_{14} and c_{15} in Table 1,

$$g^{\partial h^3 V} = -\frac{c_{14}}{2}, \quad g^{(\partial h)^4} = c_{15}. \quad (2.22)$$

In Table 2 we invert eq. (2.12)-eq. (2.22) to express the HEFT WCs as linear combinations of anomalous couplings presented in this subsection. Our final bounds on c_1 - c_{15} can be translated to bounds on the anomalous couplings using this table.

⁴This can be seen from the fact that the amplitude due to any contact term containing field strength tensors, vanishes if we approximate the longitudinal polarization vector to be $\epsilon_{L,\mu}^V = p_\mu/m_V$. Thus the true amplitude must be suppressed by powers of $(\epsilon_{L,\mu}^V - p_\mu/m_V) \sim m_V/\sqrt{s}$ and therefore cannot grow as s^2 .

HEFT Wilson coefficients	Anomalous Couplings
c_1	$-\frac{1}{2g^2} \left(\delta g_{WW1}^Q + \delta g_{WW2}^Q - 4c_{\theta_W}^2 \delta \kappa^Z - 4s_{\theta_W}^2 \delta \kappa^\gamma \right)$
c_2	$\frac{1}{g^2} \left(\delta g_{WW1}^Q - 2c_{\theta_W}^2 \delta \kappa^Z - 2s_{\theta_W}^2 \delta \kappa^\gamma \right)$
c_3	$\frac{4}{g^2} \left(c_{\theta_W}^4 \delta g_{ZZ1}^Q - \delta g_{WW1}^Q - 2c_{\theta_W}^4 \delta g_Z^1 + 2c_{\theta_W}^2 \delta \kappa^Z + 2s_{\theta_W}^2 \delta \kappa^\gamma \right)$
c_4	$\frac{2}{g^2} \left(\delta g_{WW1}^Q + \delta g_{WW2}^Q + c_{\theta_W}^4 \left(4\delta g_Z^1 - 2\delta g_{ZZ2}^Q \right) - 4c_{\theta_W}^2 \delta \kappa^Z - 4s_{\theta_W}^2 \delta \kappa^\gamma \right)$
c_5	$\frac{2}{g^2} \left(\delta g_{WW1}^Q - \delta g_{WW2}^Q + 4c_{\theta_W}^4 \left(\delta g_{ZZ2}^Q - \delta g_{ZZ1}^Q \right) + 2h_{ZZ}^Q \right)$
c_6	$g_{W3}^{\partial h V^3}$
c_7	$2g_{W2}^{\partial h V^3}$
c_8	$4g_{W1}^{\partial h V^3}$
c_9	$-2 \left(2g_{W2}^{\partial h V^3} + g_{W3}^{\partial h V^3} - 2g_Z^{\partial h V^3} \right)$
c_{10}	$-g_{W2}^{hh}$
c_{11}	$\frac{1}{2} \left(2g_{W1}^{hh} + g_{W2}^{hh} \right)$
c_{12}	$2 \left(g_{W2}^{hh} - g_{Z2}^{hh} \right)$
c_{13}	$\left(4g_{Z1}^{hh} + g_{Z2}^{hh} - 2g_{W1}^{hh} - g_{W2}^{hh} \right)$
c_{14}	$-2g^{\partial h^3 V}$
c_{15}	$g^{(\partial h)^4}$

Table 2: Mapping between the HEFT WCs for the operators in Table 1 and the anomalous couplings presented in Sec. 2.2.

2.3 SMEFT parametrization

A straightforward way to identify the SMEFT operators contributing to the gauge-Higgs scattering amplitudes is by listing the operators that generate the anomalous terms presented in the previous subsection. In the dimension-8 basis presented in Ref. [42, 43], the list of operators thus obtained can be subdivided into two groups. First the three dimension

8 operators,

$$\mathcal{O}_{s1} = \left[(D_\mu H)^\dagger (D_\nu H) \right] \left[(D^\mu H)^\dagger (D^\nu H) \right], \quad (2.23)$$

$$\mathcal{O}_{s2} = \left[(D_\mu H)^\dagger D^\mu H \right]^2, \quad (2.24)$$

$$\mathcal{O}_{s3} = \left[(D_\mu H)^\dagger (D_\nu H) \right] \left[(D^\nu H)^\dagger (D^\mu H) \right]. \quad (2.25)$$

directly generate vertices with four derivatives and four h /Goldstones, thus giving an amplitude that grows as s^2 in the forward limit. Here we have defined, $D_\mu H = \partial_\mu + ig \frac{\sigma^a W_\mu^a}{2} H + ig' Y_H B_\mu H$ where $Y_H = 1/2$ is the hypercharge of the Higgs doublet. In addition, the following five operators generating corrections to vector boson scattering via input parameter shifts, contributions to the gauge kinetic terms or by directly generating aQGCs,

$$\mathcal{O}_T = \frac{1}{2} (H^\dagger \overleftrightarrow{D}_\mu H)^2, \quad (2.26)$$

$$\mathcal{O}_{WB} = gg' (H^\dagger \sigma^a H) W_{\mu\nu}^a B^{\mu\nu}, \quad (2.27)$$

$$\mathcal{O}_U = g^2 (H^\dagger \sigma^a H) (H^\dagger \sigma^d H) W_{\mu\nu}^a W^{b,\mu\nu}, \quad (2.28)$$

$$\mathcal{O}_{H^2T} = \frac{1}{2} (H^\dagger H) (H^\dagger \overleftrightarrow{D}_\mu H)^2, \quad (2.29)$$

$$\mathcal{O}_{H^2WB} = gg' (H^\dagger H) (H^\dagger \sigma^a H) W_{\mu\nu}^a B^{\mu\nu}. \quad (2.30)$$

As expected from the goldstone boson equivalence theorem, these operators do not give rise to s^2 growth in the forward amplitude once we include all the vertices they generate in the unitary gauge. We will show this explicitly in Appendix A.

We now obtain the contributions to the anomalous couplings in Sec. 2.2 from the SMEFT operators listed above. First the TGCs receive the contributions,

$$\begin{aligned} \delta g_Z^1 &= \frac{1}{2s_{\theta_w}^2} \frac{\delta m_Z^2}{m_Z^2}, \quad \delta \kappa^\gamma = g^2 \left(\mathcal{C}_{WB} + \frac{\mathcal{C}_{H^2WB}}{4} \frac{v^2}{\Lambda^2} \right) \frac{v^2}{\Lambda^2} - g^2 \mathcal{C}_U \frac{v^4}{\Lambda^4}, \\ \delta \kappa^Z &= \frac{1}{2s_{\theta_w}^2} \frac{\delta m_Z^2}{m_Z^2} - g^2 t_{\theta_w}^2 \left(\mathcal{C}_{WB} + \frac{\mathcal{C}_{H^2WB}}{4} \frac{v^2}{\Lambda^2} \right) \frac{v^2}{\Lambda^2} - g^2 \mathcal{C}_U \frac{v^4}{\Lambda^4} \end{aligned} \quad (2.31)$$

where \mathcal{C}_i is the WC of the SMEFT operator, \mathcal{O}_i , and,

$$\frac{\delta m_Z^2}{m_Z^2} = - \left(\mathcal{C}_T + \frac{\mathcal{C}_{H^2T}}{2} \frac{v^2}{\Lambda^2} \right) \frac{v^2}{\Lambda^2} + 2g^2 t_{\theta_w}^2 \left(\mathcal{C}_{WB} + \frac{\mathcal{C}_{H^2WB}}{2} \frac{v^2}{\Lambda^2} \right) \frac{v^2}{\Lambda^2} + g^2 \mathcal{C}_U \frac{v^4}{\Lambda^4}$$

Next the aQGCs get the following contribution from the SMEFT operators,

$$\begin{aligned} \delta g_{ZZ1}^Q &= \frac{1}{s_{\theta_w}^2} \frac{\delta m_Z^2}{m_Z^2} + \frac{g^2}{16c_{\theta_w}^4} \frac{v^4}{\Lambda^4} (\mathcal{C}_{s1} + \mathcal{C}_{s3}), \quad \delta g_{ZZ2}^Q = \frac{1}{s_{\theta_w}^2} \frac{\delta m_Z^2}{m_Z^2} - \frac{g^2}{16c_{\theta_w}^4} \frac{v^4}{\Lambda^4} \mathcal{C}_{s2}, \\ \delta g_{WW1}^Q &= \frac{c_{\theta_w}^2}{s_{\theta_w}^2} \frac{\delta m_Z^2}{m_Z^2} + \frac{g^2}{8} \frac{v^4}{\Lambda^4} \mathcal{C}_{s1} - 2g^2 \mathcal{C}_U \frac{v^4}{\Lambda^4}, \quad \delta g_{WW2}^Q = \frac{c_{\theta_w}^2}{s_{\theta_w}^2} \frac{\delta m_Z^2}{m_Z^2} - \frac{g^2}{8} \frac{v^4}{\Lambda^4} (\mathcal{C}_{s2} + \mathcal{C}_{s3}) - 2g^2 \mathcal{C}_U \frac{v^4}{\Lambda^4}, \\ h_{ZZ}^Q &= \frac{g^2}{16} \frac{v^4}{\Lambda^4} (\mathcal{C}_{s1} + \mathcal{C}_{s2} + \mathcal{C}_{s3}). \end{aligned} \quad (2.32)$$

Finally, for the anomalous couplings of the forms, $(\partial h)^2 V^2$, $(\partial h)V^3$, $(\partial h)^3 V$ and $(\partial h)^4$, we respectively obtain,

$$\begin{aligned}\delta g_{Z1}^{hh} &= -\frac{1}{8}(\mathcal{C}_{s1} - \mathcal{C}_{s2} - \mathcal{C}_{s3})\frac{v^4}{\Lambda^4}, & \delta g_{Z2}^{hh} &= \frac{\mathcal{C}_{s1}}{2}\frac{v^4}{\Lambda^4}, \\ \delta g_{W1}^{hh} &= \frac{\mathcal{C}_{s2}}{4}\frac{v^4}{\Lambda^4}, & \delta g_{W2}^{hh} &= \frac{\mathcal{C}_{s1} + \mathcal{C}_{s3}}{4}\frac{v^4}{\Lambda^4},\end{aligned}\quad (2.33)$$

$$g_{W1}^{\partial h V^3} = \frac{1}{4}(\mathcal{C}_{s3} - \mathcal{C}_{s1})\frac{v^4}{\Lambda^4}, \quad g_{W2}^{\partial h V^3} = 0, \quad g_{W3}^{\partial h V^3} = 0, \quad g_Z^{\partial h V^3} = 0, \quad (2.34)$$

and,

$$g^{\partial h^3 V} = 0, \quad g^{(\partial h)^4} = \frac{1}{4}(\mathcal{C}_{s1} + \mathcal{C}_{s2} + \mathcal{C}_{s3})\frac{v^4}{\Lambda^4}. \quad (2.35)$$

In eq. (2.32)-eq. (2.35), the total number of anomalous coupling on the left hand side (18) is larger than the number of independent SMEFT contributions (6) on the right hand side.⁵ This implies that the anomalous couplings must satisfy 12 constraints in the dimension-8 SMEFT that can be obtained in a straightforward way by eliminating the SMEFT WCs from eq. (2.32)-eq. (2.35). These constraints, expressed in terms of HEFT WCs, have been shown in Table 3.

These constraints imply that in the space of the 15 HEFT WCs of Table 1, the SMEFT is a three dimensional hyperplane. We will see that the SMEFT positivity bounds obtained in past literature can be recovered by obtaining a projection of our 15 dimensional bounds derived in Sec. on the 3 dimensional SMEFT plane using Table 3.

Finally we mention a few subtleties before proceeding further. First of all the constraints obtained in Table 3 will be broken by higher dimension operators suppressed by additional powers of the cutoff. We assume the following power-counting for the SMEFT WCs,

$$\text{SMEFT} : \frac{\Lambda^4}{g_H^2} \left(\frac{D}{\Lambda}\right)^{n_D} \left(\frac{g_H H}{\Lambda}\right)^{n_H} \quad (2.36)$$

where, $g_H < \Lambda/v$, is the coupling of the Higgs to heavy BSM states. The contribution of higher dimensional WCs to the scattering amplitudes relative to that of dimensional-8 ones is therefore suppressed by powers of $g_H^2 v^2/\Lambda^2$. We see that in the limit $g_H \rightarrow \Lambda/v$ this suppression vanishes and indeed the SMEFT power counting in eq. (2.36) approaches the HEFT power counting in eq. (2.7). This is, however, exactly the limit in which the SMEFT expansion breaks down and the correct effective description is given by HEFT. A second subtlety is that if we assume the power counting scheme in eq. (2.36), the contribution of diagrams with two insertions of dimension-6 operators cannot be ignored for a g_H that is $\mathcal{O}(1)$. Fortunately, however, the dimension-6 contributions have been found to give a negative definite contribution [13, 14] to the s^2 piece of the forward amplitude so that individual bounds can still be placed on the dimension-8 contribution. Thus in our list above we have only included SMEFT operators that contribute to gauge-Higgs scattering with a single insertion.

⁵Note that the WCs $\mathcal{C}_T, \mathcal{C}_{H^2 T}$ ($\mathcal{C}_{WB}, \mathcal{C}_{H^2 WB}$) always appear in these equations in the same linear combination, $\mathcal{C}_T + \frac{\mathcal{C}_{H^2 T} v^2}{2\Lambda^2}$ ($\mathcal{C}_{WB} + \frac{\mathcal{C}_{H^2 WB} v^2}{2\Lambda^2}$).

SMEFT Constraints
$c_3 + c_4 = 0$
$c_5 = 0$
$16c_1 - 2c_{10} - 4c_{11} - c_{12} - 2c_{13} = 0$
$c_{10} + c_{12}/2 + 4c_2 = 0$
$4c_1 - c_{10}/2 - c_{11} + c_4 = 0$
$c_{10} + 4c_2 + c_3 = 0$
$4c_3 - c_8 = 0$
$c_6, c_7, c_9 = 0$
$c_{14} = 0$
$4(c_1 + c_2) - c_{15} = 0$

Table 3: Linear constraints on the WCs of NLO HEFT operators implied by the SMEFT truncated at dimension-8 level.

2.4 Longitudinal gauge-Higgs scattering amplitude

We now present the amplitude for longitudinal gauge-Higgs scattering, $b_i b_j \rightarrow b_k b_l$ with the indices taking values from 1–4 and $b = \{W_{1L}, W_{2L}, Z_L, h\}$. We will show using only $U(1)_{em}$ invariance that the coefficient of s^2 in the forward amplitude can be parametrized by 15 independent parameters. We will then provide an explicit mapping between these parameters and the 15 HEFT WCs—or equivalently the 15 linear combinations of anomalous couplings in Table 2.

We separate the full gauge-Higgs scattering amplitude into two parts,

$$\mathcal{M}_{ijkl}^V(s, t) = \mathcal{M}_{ijkl}^{V, sing}(s, t) + \tilde{\mathcal{M}}_{ijkl}^V(s, t) \quad (2.37)$$

where the first term contains all the IR singularities from tree-level exchange of light particles in the s, t or u channel as well as loop contributions. For the goldstone scattering amplitude, $\phi_i \phi_j \rightarrow \phi_k \phi_l$, we can similarly subtract out the IR singularities to obtain $\tilde{\mathcal{M}}_{ijkl}^\phi$. The goldstone boson equivalence theorem implies, $\tilde{\mathcal{M}}_{ijkl}^V = \tilde{\mathcal{M}}_{ijkl}^\phi$ for $s \gg m_{h,W,Z}^2$ which allows us to drop the superscripts and simply use $\tilde{\mathcal{M}}_{ijkl}$ to denote the amplitude. In the UV, $s > \Lambda^2$, $\tilde{\mathcal{M}}_{ijkl}$ gives the exact amplitude. For $m_{h,W,Z}^2 \ll s, t \ll \Lambda^2$ we can expand the second term in powers of s and t as follows,

$$\tilde{\mathcal{M}}_{ijkl}(s, t) = \sum_{m,n} c_{ijkl}^{m,n} s^m t^n \quad (2.38)$$

where we have assumed that the tree-level HEFT contribution is a good approximation for the low-energy amplitude.⁶ For the purpose of deriving the positivity bounds in this work

⁶See Ref. [19, 44, 45] for a discussion about the effect of EFT-loops on positivity bounds.

we require only, $c_{ijkl}^{2,0}$.

Before producing a mapping between the, $c_{ijkl}^{2,0}$, and the HEFT WCs let us first count the number of independent, $c_{ijkl}^{2,0}$, imposing only $U(1)_{em}$ invariance. As the $U(1)_{em}$ acts like an $SO(2)$ on the indices, $i = 1, 2$, we write the amplitude, \mathcal{M}_{ijkl} , using invariant tensors of the $SO(2)$ symmetry group,

$$\tilde{\mathcal{M}}_{ijkl} = \delta_{ij}\delta_{kl} f(s, u) + \delta_{ik}\delta_{jl} f(t, u) + \delta_{il}\delta_{kj} f(u, s) \quad \text{for } i, j, k, l \in [1, 2], \quad (2.39)$$

where, the function $f(s, u)$ is symmetric under exchange of s and u . The form of the amplitude in eq. (2.39) implies the following constraints,

$$\tilde{\mathcal{M}}_{1111}(s) = \tilde{\mathcal{M}}_{2222}(s) \quad (2.40)$$

$$\tilde{\mathcal{M}}_{1111}(s) = \tilde{\mathcal{M}}_{1212}(s) + \tilde{\mathcal{M}}_{1221} + \tilde{\mathcal{M}}_{1122}(s). \quad (2.41)$$

For 2-to-2 scattering amplitudes involving Z_L and h (or ϕ_3 and h for the corresponding goldstone amplitude), $U(1)_{em}$ invariance implies $\tilde{\mathcal{M}}_{12ii}^V = \tilde{\mathcal{M}}_{1ii2}^V = \tilde{\mathcal{M}}_{1i2i}^V = 0$, $\tilde{\mathcal{M}}_{1i1i}^V = \tilde{\mathcal{M}}_{2i2i}^V$, $\tilde{\mathcal{M}}_{11ii}^V = \tilde{\mathcal{M}}_{22ii}^V$ and $\tilde{\mathcal{M}}_{1ii1}^V = \tilde{\mathcal{M}}_{2ii2}^V$ where $i = 3, 4$.

These constraints can be directly translated to the, $c_{ijkl}^{2,0}$, given by,

$$c_{ijkl}^{2,0} = \left. \frac{1}{2} \frac{\partial^2 \tilde{\mathcal{M}}_{ijkl}}{\partial s^2} \right|_{s,t=0}. \quad (2.42)$$

They would imply that many of the $c_{ijkl}^{2,0}$ are equal to each other and many others vanish. In matrix form we can write,

$$v^4 c_{ijkl}^{2,0} = \begin{pmatrix} a_1 & 0 & 0 & 0 & a_2 & 0 & 0 & 0 & a_3 & 0 & 0 & a_9 & 0 & 0 & a_9 & a_{12} \\ 0 & a_4 & 0 & a_2 & 0 & 0 & 0 & 0 & 0 & 0 & 0 & -a_{16} & 0 & 0 & a_{16} & 0 \\ 0 & 0 & a_6 & 0 & 0 & 0 & a_3 & 0 & 0 & a_{10} & 0 & 0 & a_9 & a_{16} & 0 & 0 \\ 0 & a_2 & 0 & a_4 & 0 & 0 & 0 & 0 & 0 & 0 & 0 & a_{16} & 0 & 0 & -a_{16} & 0 \\ a_2 & 0 & 0 & 0 & a_1 & 0 & 0 & 0 & a_3 & 0 & 0 & a_9 & 0 & 0 & a_9 & a_{12} \\ 0 & 0 & 0 & 0 & 0 & a_6 & 0 & a_3 & 0 & 0 & a_{10} & 0 & -a_{16} & a_9 & 0 & 0 \\ 0 & 0 & a_3 & 0 & 0 & 0 & a_6 & 0 & 0 & a_9 & a_{16} & 0 & a_{10} & 0 & 0 & 0 \\ 0 & 0 & 0 & 0 & 0 & a_3 & 0 & a_6 & 0 & -a_{16} & a_9 & 0 & 0 & a_{10} & 0 & 0 \\ a_3 & 0 & 0 & 0 & a_3 & 0 & 0 & 0 & a_5 & 0 & 0 & a_7 & 0 & 0 & a_7 & a_8 \\ 0 & 0 & a_{10} & 0 & 0 & 0 & a_9 & -a_{16} & 0 & a_{14} & 0 & 0 & a_{12} & 0 & 0 & 0 \\ 0 & 0 & 0 & 0 & 0 & a_{10} & a_{16} & a_9 & 0 & 0 & a_{14} & 0 & 0 & a_{12} & 0 & 0 \\ a_9 & -a_{16} & 0 & a_{16} & a_9 & 0 & 0 & 0 & a_7 & 0 & 0 & a_{13} & 0 & 0 & a_{15} & a_{11} \\ 0 & 0 & a_9 & 0 & 0 & -a_{16} & a_{10} & 0 & 0 & a_{12} & 0 & 0 & a_{14} & 0 & 0 & 0 \\ 0 & 0 & a_{16} & 0 & 0 & a_9 & 0 & a_{10} & 0 & 0 & a_{12} & 0 & 0 & a_{14} & 0 & 0 \\ a_9 & a_{16} & 0 & -a_{16} & a_9 & 0 & 0 & 0 & a_7 & 0 & 0 & a_{15} & 0 & 0 & a_{13} & a_{11} \\ a_{12} & 0 & 0 & 0 & a_{12} & 0 & 0 & 0 & a_8 & 0 & 0 & a_{11} & 0 & 0 & a_{11} & a_{15} \end{pmatrix}$$

where the rows and columns are ordered as follows,

$$\{11, 12, 13, 21, 22, 23, 31, 32, 33, 14, 24, 34, 41, 42, 43, 44\} \quad (2.43)$$

and respectively denote different possible initial and final states for gauge-Higgs scattering. For instance, the top left entry a_1 corresponds to either the $W_{1L}W_{1L} \rightarrow W_{1L}W_{1L}$. Our parametrization in terms of the $a_1 - a_{16}$ already incorporates all the constraints arising from $U(1)_{em}$ apart from eq. (2.41) which implies the relation,

$$a_1 = 2a_2 + a_4. \quad (2.44)$$

There are thus 15 independent parameters required to completely parametrize the s^2 piece of the forward amplitude.⁷

We now proceed to calculate the amplitude, $\tilde{\mathcal{M}}_{ijkl}$, using the lagrangians presented in the previous subsections. We can either use the unitary gauge parametrization of Sec. 2.2 or the HEFT parametrization in Sec. 2.1 to obtain the matrix in eq. (2.43). We carry out both these computations and explicitly verify that they yield the same answer. We find,

$$\begin{aligned} a_1 &= 16(c_1 + c_2), & a_2 &= 4(2c_1 + c_2), & a_3 &= 8c_1 + 4c_2 + c_3 + 2c_4 \\ a_4 &= 8c_2, & a_5 &= 16(c_1 + c_2) + 8(c_3 + c_4) + 4c_5, & a_6 &= 2(4c_2 + c_3) \\ a_7 &= 2c_6 + 2c_7 + c_9, & a_8 &= 2c_{11} + c_{13}, & a_9 &= c_6 + \frac{c_7}{2}, & a_{10} &= c_7 \\ a_{11} &= -\frac{c_{14}}{2}, & a_{12} &= 2c_{11}, & a_{13} &= -2c_{10} - c_{12}, & a_{14} &= -2c_{10}, \\ a_{15} &= 4c_{15}, & a_{16} &= \frac{c_8}{4}. \end{aligned} \quad (2.45)$$

We see that eq. (2.45) clearly satisfies eq. (2.44) and thus provides a one-to-one mapping between the 15 independent parameters of the amplitude and the 15 HEFT WCs—and hence the 15 linear combination of the anomalous couplings in Table 2

Finally note that from eq. (2.45) it is clear that the $c_{ijkl}^{2,0}$ get no contribution from the HEFT WCs in eq. (2.11) (and thus no contribution from the SMEFT WCs in eq. (2.26)). While this fact is trivial for goldstone scattering, $\phi_i\phi_j \rightarrow \phi_k\phi_l$ it is, far from obvious in the unitary gauge calculation involving anomalous couplings. We, therefore, carry out the latter calculation explicitly in Appendix A.

3 The positivity cone: analytical positivity constraints

In this section we derive analytical positivity bounds on the operators in Table 1. Our starting point would be the twice-subtracted dispersion relation for longitudinal gauge-Higgs scattering at a fixed t . In order to derive this we assume that for a given t , $\tilde{\mathcal{M}}_{ij}(s, t)$ defined in eq. (2.37) is an analytic function in the complex s -plane apart from s and u -channel singularities on the real line due to new states at $s \geq \Lambda^2$ and $u \geq \Lambda^2$. We also make use of the Froissart-Martin bound [46, 47] which not only restricts the high energy behavior of the full amplitude but can also be applied directly to $\tilde{\mathcal{M}}_{ij}(s, t)$. This is because of the fact that in the HEFT at NLO, the residue of t -channel poles below the cutoff has at most a

⁷Note that the coefficients of st and t^2 in $\tilde{\mathcal{M}}_{ijkl}$ are related to the $c_{ijkl}^{2,0}$ by crossing-symmetry and are thus not independent. Thus we need only 15 parameters to parametrize all the $c_{ijkl}^{m,n}$ with $m + n = 2$.

linear dependence on s .⁸ Finally, we use $\tilde{\mathcal{M}}_{ijkl}(s+i\epsilon, t) = \tilde{\mathcal{M}}_{ijkl}^*(m_{ijkl}^2 - s - i\epsilon - t, t)$ which follows from su -crossing symmetry and real-analiticity where $m_{ijkl}^2 = m_i^2 + m_j^2 + m_k^2 + m_l^2$. We can then use the standard procedure to obtain the dispersion relation (see for eg. Ref. [48]),

$$\begin{aligned} \tilde{\mathcal{M}}_{ijkl} &= a_{ijkl}^{(0)}(t) + a_{ijkl}^{(1)}(t)s \\ &+ \frac{(s-s_*)^2}{2\pi i} \int_{\Lambda^2}^{\infty} ds' \frac{1}{(s'-s_*)^2} \left(\frac{\text{Disc } \tilde{\mathcal{M}}_{ijkl}(s', t)}{(s'-s)} + \frac{\text{Disc } \tilde{\mathcal{M}}_{ilkj}(s', t)}{(s'-u)} \right) \end{aligned} \quad (3.1)$$

where $\text{Disc } M_{ijkl} = \lim_{\epsilon \rightarrow 0^+} \mathcal{M}_{ijkl}(s+i\epsilon, t) - \mathcal{M}_{ijkl}(s-i\epsilon, t)$ and s_* is an arbitrary subtraction point that we will choose to be $s_* = t/2 - m_{ijkl}^2$.

To derive positivity constraints of the kind derived in Ref. [3], it is enough to consider the $ij \rightarrow ij$ process in the forward limit, $t \rightarrow 0$. We can then use the optical theorem, $\text{Disc } M_{ijij} = 2i \text{Im} M_{ijij} = \sqrt{(s' - (m_{ij}^+)^2)(s' - (m_{ij}^-)^2)} \sigma_{ij}(s')$ and eq. (3.1) to obtain for the forward amplitude $\tilde{\mathcal{M}}_{ij}(s) = \tilde{\mathcal{M}}_{ijij}(s, t \rightarrow 0)$,

$$\frac{1}{2} \frac{\partial^2}{\partial s^2} \tilde{\mathcal{M}}_{ij}(s) = \frac{1}{\pi} \int_{\Lambda^2}^{\infty} ds' \sqrt{(s' - (m_{ij}^+)^2)(s' - (m_{ij}^-)^2)} \sigma_{ij}(s') \left[\frac{1}{(s' - s)^3} \right. \quad (3.2)$$

$$\left. + \frac{1}{(s' - (m_{ij}^+)^2 + s)^3} \right] \quad (3.3)$$

where the right hand side is clearly positive. Here, we have defined $m_{ij}^{\pm} = m_i \pm m_j$. We can immediately use the above equation to obtain our first set of positivity bounds by demanding that the diagonal elements of the matrix in eq. (2.43) are positive.

More optimal bounds can be obtained, by considering the scattering of the quantum superposed states, $|\alpha\rangle = \alpha_i|i\rangle$, $|\beta\rangle = \beta_j|j\rangle$,

$$|\alpha; k_1\rangle + |\beta; k_2\rangle \rightarrow |\alpha; k_3\rangle + |\beta; k_4\rangle. \quad (3.4)$$

which has the following amplitude,

$$\tilde{\mathcal{M}}_{\alpha\beta \rightarrow \alpha\beta}(s, t) = \sum_{i,j,k,l=1}^3 \alpha_i \beta_j \alpha_k^* \beta_l^* \tilde{\mathcal{M}}_{ijkl}(s, t) \quad (3.5)$$

Using the arguments that led to eq. (3.3) we now infer,

$$\frac{\partial^2}{\partial s^2} \tilde{\mathcal{M}}_{\alpha\beta \rightarrow \alpha\beta}(s, t \rightarrow 0)|_{s=0} = \sum_{i,j,k,l=1}^3 \alpha_i \beta_j \alpha_k^* \beta_l^* \frac{\partial^2}{\partial s^2} \tilde{\mathcal{M}}_{ijkl}(s, t \rightarrow 0)|_{s=0} > 0 \quad (3.6)$$

⁸The photon exchange diagrams may still seem problematic as they blow up in the $t \rightarrow 0$ limit. One can, however, circumvent this issue because positivity arguments also hold away from the forward limit for a small but finite t .

This implies that the matrix,

$$(\gamma_\beta)_{ik} = \beta_j \beta_l^* \frac{\partial^2}{\partial s^2} \tilde{\mathcal{M}}_{ijkl}(s, t \rightarrow 0)|_{s=0} \quad (3.7)$$

is a positive definite hermitian matrix which in turn requires that all its principal minors must be positive. In particular, we can demand the positivity of all the diagonal entries of $(\gamma_\beta)_{ik}$ as well as the determinant of all principal 2×2 sub-matrices. This yields the 10 conditions presented in Appendix B that depend on the β_i in eq. (3.7). In Appendix B we show how the β_i can be optimally chosen to obtain the 16 positivity constraints presented in Table 4.

In the upper block of Table 4 we present the first set of positivity constraints obtained from requiring the positivity of the diagonal elements of γ_β . These constraints involve only the CP even WCs, c_{1-5}, c_{10}, c_{12} , and c_{15} , that contribute to the elastic scattering processes, $V_L h \rightarrow V_L h$, $Z_L Z_L \rightarrow Z_L Z_L$, $W_L W_L \rightarrow W_L W_L$, $W_L Z_L \rightarrow W_L Z_L$ and $hh \rightarrow hh$. Positivity bounds on the CP-odd WCs or even the CP-even ones contributing to the inelastic processes, $V_L V_L, hh \rightarrow V_L h$, arise from the second set of constraints obtained by requiring the positivity of the determinants of the 2×2 principal sub-matrices; these have been presented in the lower block of Table 4. The second set of constraints has the form, $A^2 < BC$, where B and C are linear combinations of CP-even WCs contributing to elastic processes—that are already required to be positive by the first set of positivity constraints—and A is a linear combination that includes CP-odd couplings and WCs contributing to $V_L V_L, hh \rightarrow V_L h$. The second set of conditions thus imply that all CP-odd couplings and all the WCs contributing to $V_L V_L, hh \rightarrow V_L h$ must vanish if the other WCs vanish. This also implies that theoretical or experimental bounds on the CP even couplings contributing to the elastic processes imply upper bounds on the magnitude of the CP-odd couplings and the WCs contributing to the inelastic processes, $V_L V_L, hh \rightarrow V_L h$ —a fact that we will use to compute our final positivity constraints in Sec. 5.

Let us now compare bounds obtained in Table 4 with existing literature. Some positivity constraints on the electroweak chiral Lagrangian were earlier explored in Ref. [23, 24]. The first two inequalities presented in Table 4 are consistent with the results of these studies. Furthermore, positivity constraints on the SMEFT lagrangian have been derived in Ref. [13–15]. We can recover the SMEFT positivity constraints by expressing the HEFT WCs in terms of the SMEFT ones as follows,

$$c_1 = \frac{1}{16}(\mathcal{C}_{s3} + \mathcal{C}_{s2} - \mathcal{C}_{s1}) \frac{v^4}{\Lambda^4}, \quad c_2 = \frac{\mathcal{C}_{s1}}{8} \frac{v^4}{\Lambda^4}, \quad c_3 = \frac{\mathcal{C}_{s3} - \mathcal{C}_{s1}}{4} \frac{v^4}{\Lambda^4} = -c_4, \quad c_5 = 0,$$

where Λ denotes the cutoff scale. Using the above equation and Table 4, we can derive the following constraints on the SMEFT parameter space:

$$\mathcal{C}_{s1} > 0, \quad \mathcal{C}_{s1} + \mathcal{C}_{s3} > 0, \quad \mathcal{C}_{s1} + \mathcal{C}_{s2} + \mathcal{C}_{s3} > 0. \quad (3.8)$$

This reproduces the bounds reported in [14]. As shown in Ref. [14], contributions to the scattering amplitudes from two dimension-6 insertions do not invalidate the above bounds as they turn out to be negative definite.

Set 1
$c_2 > 0$
$c_1 + c_2 > 0$
$4(c_1 + c_2) + 2(c_3 + c_4) + c_5 > 0$
$4c_2 + c_3 > 0$
$c_{10} < 0$
$2c_{10} + c_{12} < 0$
$c_{15} > 0$
Set 2
$4a_3^2 < (a_6 + \sqrt{a_1 a_5})^2$
$a_9^2 < a_6 a_{11}$
$a_{12}^2 < a_5 a_{13}$
$a_{15}^2 < a_{13} a_{16}$
$4a_7^2 < (\sqrt{a_{11} a_6} + \sqrt{a_{13} a_1})^2$
$4a_{10}^2 < (\sqrt{a_6 a_{11}} + \sqrt{a_4 a_{13}})^2$
$4a_8^2 < (a_{11} + \sqrt{a_1 a_{16}})^2$
$(a_{12} + a_{15} + 2a_{14})^2 < (a_5 + a_{13} + 2a_{12})(a_{13} + a_{16} + 2a_{15})$

Table 4: Positivity constraints on the HEFT WCs in Table 1. These constraints can be translated to constraints on the anomalous couplings contributing to longitudinal gauge-Higgs scattering using the mapping presented in Table 2. Here $a_1 = 16(c_1 + c_2)$, $a_2 = 4(2c_1 + c_2)$, $a_3 = 8c_1 + 2c_2 + c_3 + 4c_4$, $a_4 = 8c_2$, $a_5 = 16(c_1 + c_2) + 8(c_3 + c_4) + 4c_5$, $a_6 = 2(4c_2 + c_3)$, $a_7 = c_6 + \frac{c_7}{2}$, $a_8 = 2c_{11}$, $a_9 = c_7$, $a_{10} = -\frac{c_8}{4}$, $a_{11} = -2c_{10}$, $a_{12} = 2(c_6 + c_7 + c_9/2)$, $a_{13} = -(2c_{10} + c_{12})$, $a_{14} = (2c_{11} + c_{13})$, $a_{15} = -c_{14}/2$, $a_{16} = 4c_{15}$.

Together, the constraints in Table 4 give an allowed region that forms a convex cone [22] in the space of WCs. Note that the positive definiteness of γ_β implies further constraints in addition to those in Table 4 as we can further demand,

$$\begin{aligned} \det(\gamma_{\mathbf{3}\beta}) &> 0 \\ \det(\gamma_\beta) &> 0 \end{aligned} \tag{3.9}$$

where $\gamma_{\mathbf{3}\beta}$ is the submatrix of γ_β obtained by removing the fourth row and column. These conditions must hold for an arbitrary choice of the β_i . It is, however, not straightforward to optimally choose the β_i to get analytical bounds. We will not explore these two conditions further as the numerical methods discussed in the next section provide an alternative way to derive the positivity cone that includes the implications of both Table 4 and eq. (3.9). Furthermore, they also provide double-sided bounds on the WCs that close this conical allowed region. In the coming sections we will refer to the region in the HEFT space

consistent with Table 4 as the ‘HEFT positivity cone’ and the region defined by eq. (3.8) as the ‘SMEFT positivity cone’.

4 Capping the positivity cone: double sided bounds from s - t crossing and unitarity.

In the previous section we derived the positivity bounds summarized in Table 4 and eq. (3.9). In order to derive these constraints, we used su crossing symmetry but did not impose st crossing symmetry. As we will discuss shortly, the full implications of unitarity were also not applied in Sec. 3.3. These additional conditions can be imposed using the numerical methods developed in [8, 9, 18, 49], that result in double-sided bounds on EFT WCs. We will now show how these methods can be used to close the conical allowed region obtained in the previous section. To use the terminology introduced in Ref. [18, 49] these numerical methods allow us to ‘cap the positivity cone’(from here on we will sometimes refer to these numerical bounds as ‘capping bounds’. We will carry out this procedure for the WCs contributing to the $V_L V_L \rightarrow V_L V_L$, hh and $hh \rightarrow hh$ processes. Below, we briefly outline the procedure; for further details, please see [18] and references therein.

IR-UV relations First, let us recast eq. (3.1) in terms of the new variable, $v = s + t/2 + m_{ijkl}^2/2 = -u - t/2 - m_{ijkl}^2/2$,

$$\tilde{\mathcal{M}}_{ijkl} = \tilde{a}_{ijkl}^{(0)}(t) + \tilde{a}_{ijkl}^{(1)}(t)v + \frac{(s - s_\star)^2}{2\pi i} \int_{\Lambda^2}^{\infty} ds' \frac{1}{(s' - s_\star)^2} \left(\frac{\text{Disc} \tilde{\mathcal{M}}_{ijkl}(s', t)}{(s' - s)} + \frac{\text{Disc} \tilde{\mathcal{M}}_{ilkj}(s', t)}{(s' - u)} \right) \quad (4.1)$$

and also rewrite the low-energy expansion for the EFT amplitude in terms of t and the new variable v ,

$$\tilde{\mathcal{M}}_{ijkl}(s, t) = \sum_{m,n} \tilde{c}_{ijkl}^{m,n} v^m t^n. \quad (4.2)$$

Taking $m \geq 2$ derivatives with respect to v and n derivatives with respect to t , we obtain,

$$\tilde{c}_{ijkl}^{m,n} = \left\langle \left[\rho_l^{ijkl}(s') + (-1)^m \rho_l^{ilkj}(s') \right] \sum_{p=0}^n \frac{L_l^p H_{m+1}^{n-p}}{s'^{m+n+1}} \right\rangle \quad (4.3)$$

where ρ_l^{ijkl} are the ‘spectral densities’ obtained from the partial wave expansion of the absorptive part of the high energy amplitude,

$$\frac{1}{2i} \text{Disc} \tilde{\mathcal{M}}_{ijkl}(\mu, t) = 16\pi \sum_{l=0}^{\infty} (2l+1) P_l \left(1 + \frac{2t}{\mu} \right) \rho_l^{ijkl}(\mu). \quad (4.4)$$

P_l are the Legendre polynomials and we have used the notation of Ref. [18], where,

$$\langle \dots \rangle = \sum_l 16(2l+1) \int_{\Lambda^2}^{\infty} ds' (\dots) \quad (4.5)$$

and,

$$L_l^n = \frac{\Gamma(l+n+1)}{n!\Gamma(l-n+1)\Gamma(n+1)}, H_{m+1}^q = \frac{\Gamma(m+q+1)}{(-2)^q\Gamma(q+1)\Gamma(m+1)}. \quad (4.6)$$

Eq. (4.3) relates the the low-energy EFT amplitude to the spectral densities, ρ_l^{ijkl} , which encode UV dynamics. Note that with our assumption that EFT loops can be neglected, the HEFT WCs can be written as linear combinations of the \tilde{c}_{ijkl}^{mn} . We can thus find their allowed range by varying the spectral densities in the range allowed by unitarity. Apart from unitarity constraints, the spectral densities must also satisfy the so-called null-constraints that arise from st -crossing, and symmetry constraints implied by the unbroken $U(1)_{em}$. Note that the positivity constraints derived in the last section arise from the fact that for certain linear combinations of the $\tilde{c}_{ijkl}^{m,n}$ in eq. (4.3), the right hand side can be related to a cross-section by the optical theorem. Therefore, the analytical positivity constraints of Table 4 would be automatically satisfied by the allowed region obtained using the numerical procedure described in this section.

Null constraints We now derive the consequences of imposing st crossing symmetry on the space of WCs and thus on the spectral densities. For the EFT amplitude in eq. (2.38), st crossing would imply,

$$c_{ijkl}^{mn} = c_{ikjl}^{nm}. \quad (4.7)$$

By relating the expansions in eq. (2.38) and eq. (4.2) we can rewrite the above condition in terms of the $\tilde{c}_{ijkl}^{m,n}$ to obtain,

$$\mathcal{N}_{ijkl}^{m,n} = \sum_{a=m}^{m+n} \frac{\Gamma(a+1)\tilde{c}_{ijkl}^{a,m+n-a}}{2^{a-m}\Gamma(m+1)\Gamma(a-m+1)} - \sum_{a=n}^{m+n} \frac{\Gamma(a+1)\tilde{c}_{ikjl}^{a,m+n-a}}{2^{a-n}\Gamma(n+1)\Gamma(a-n+1)} = 0 \quad (4.8)$$

Now one can substitute $\tilde{c}_{ijkl}^{m,n}$ s in eq. (4.8) in terms of ρ_l^{ijkl} s using eq. (4.3). to obtain the first set of null constraints on the spectral densities [8, 9]. A second set of null constraints can be derived by noting that su -crossing symmetry implies

$$\tilde{c}_{ijkl}^{1,n} + \tilde{c}_{ilkj}^{1,n} = 0. \quad (4.9)$$

Although $\tilde{c}^{1,n}$ cannot be directly connected to the spectral densities via eq. (4.1), the first set of null constraints allows us to write them in terms of $\tilde{c}^{m \geq 2, n'}$ s and thus can be expressed in terms of spectral densities.

Unitarity constraints In addition to the null-constraints, the spectral densities must obey unitarity constraints. The set of unitarity constraints that have been utilized in this work are the following,

$$0 \leq \rho_l^{iii}(s) \leq 2 \quad (4.10)$$

$$0 \leq \rho_l^{ijij}(s) \leq \frac{1}{2} \quad (4.11)$$

$$-1 \leq \rho_l^{iijj}(s) \leq 1 \quad (4.12)$$

$$|\rho_i^{iijj}(s)| \leq 1 - \left| 1 - \frac{\rho_l^{iii}(s) + \rho_l^{jjjj}(s)}{2} \right|. \quad (4.13)$$

The above inequalities were derived and discussed in great detail in Ref. [18].

Symmetry constraints Apart from crossing symmetry and unitarity, we can impose additional symmetry constraints due to the unbroken $U(1)_{em}$ group. Using Eq. (4.4), it is straightforward to translate the constraints on the amplitude in eq. (2.40) and eq. (2.41) to the spectral densities,

$$\rho_l^{1111}(s) = \rho_l^{2222}(s) \quad (4.14)$$

$$\rho_l^{1111}(s) = \rho_l^{1212}(s) + \rho_l^{1221}(s) + \rho_l^{1122}(s). \quad (4.15)$$

Now, from tu -crossing symmetry, we have $\rho_l^{ijkl}(s) = (-1)^l \rho_l^{ijlk}$. This implies that ρ_l^{1111} and ρ_l^{1122} vanish for odd l and eq. (2.41) is trivially satisfied. For even l , on the other hand, we get the non trivial constraint,

$$\rho_l^{1111} - 2\rho_l^{1212} - \rho_l^{1122} = 0. \quad (4.16)$$

As far as scattering involving Z_L/ϕ_3 and h is concerned, we can again translate the results of Sec. 2.4 to constraints on the spectral densities: $\rho_l^{12ii} = \rho_l^{1ii2} = \rho_l^{1i2i} = 0$, $\rho_l^{1i1i} = \rho_l^{2i2i}$, $\rho_l^{11ii} = \rho_l^{22ii}$ and $\rho_l^{1ii1} = \rho_l^{2ii2}$ where $i = \phi_3, h$.

Linear programming We now want to numerically compute the allowed range for $\tilde{c}_{ijkl}^{m,n}$ —and thus the allowed range for HEFT WCs—by varying the UV spectral densities ρ_l^{ijkl} on the right hand side of eq. (4.3). We will also ensure that the constraints from unitarity, st crossing and $U(1)_{em}$ symmetry are respected in this process. We will treat this as an optimization problem that can be solved using linear programming methods. Specifically, we utilize the `scipy.optimize.linprog` [50] function to perform the required computations efficiently.

To facilitate this process, we discretize the UV scale s' in eq. (4.3), reducing the problem to a finite set of UV spectral densities $\rho_l^{ijkl}(s')$, which serve as the decision variables in the optimization problem. For convenience, we transform the integration variable from s' to $x = \Lambda^2/s'$ and approximate the integral over x as a finite sum where the variable x is discretized as n/N with $n = 1, 2, \dots, N$. Additionally, we impose a cut-off l_M on the sum over UV partial waves. With this, we are left with only a finite number of partial wave amplitude $\rho_l^{ijkl}(s)$ s. The values of l_M and N are chosen to be sufficiently large to ensure numerical convergence in the optimization process. With these adjustments the sum-rules in eq. (4.3) take the following form,

$$\begin{aligned} \tilde{c}_{ijkl}^{m,n} &= \sum_{l=0}^{\infty} (2l+1) \int_{\Lambda^2}^{\infty} \frac{ds'}{s'^{m+n+1}} \left[\rho_l^{ijkl}(s') + (-1)^m \rho_l^{ilkj}(s') \right] \sum_{p=0}^n L_l^p H_{m+1}^{n-p} \\ &\approx \frac{1}{\Lambda^{2(m+1)}} \sum_{l=0}^{l_M} (2l+1) \sum_{n=1}^N \frac{1}{N} \left(\frac{n}{N} \right)^{m+n-1} \left(\rho_{l,n}^{ijkl} + (-1)^m \rho_{l,n}^{ilkj} \right) \sum_{p=0}^n L_l^p H_{m+1}^{n-p}, \end{aligned} \quad (4.17)$$

where we have defined, $\rho_{l,n}^{ijkl} = \rho_l^{ijkl}(\Lambda^2 N/n)$.

Decision Variables
$\rho_{l,n}^{1111}, \rho_{l,n}^{3333}, \rho_{l,n}^{1212}, \rho_{l,n}^{1122}, \rho_{l,n}^{1133}$ for $l = 0, \dots, l_M, n = 1, \dots, N$
Objective Function
$\tilde{c}_{1111}^{2,0}, \tilde{c}_{1212}^{2,0}, \tilde{c}_{1122}^{2,0}, \tilde{c}_{1111}^{2,0}, \tilde{c}_{1313}^{2,0}$ and $\tilde{c}_{1133}^{2,0}$, defined in eq. (4.17)
Constraints
Null Constraints
$\sum_{l=0, \dots, l_M} (2l+1) \sum_{n=1}^N \frac{1}{N} \left(\frac{n}{N}\right)^{r+2} C_{r,i_r}^{iiii}(l) \rho_{l,n}^{iiii} = 0$ for $i = 1, 3$
$\sum_{l=0, \dots, l_M} (2l+1) \sum_{n=1}^N \frac{1}{N} \left(\frac{n}{N}\right)^{r+2} \left(C_{r,i_r}^{1i1i}(l) \rho_{l,n}^{1i1i} + C_{r,i_r}^{11ii}(l) \rho_{l,n}^{11ii} \right) = 0$ for $i = 2, 3$
Unitarity Constraints
$0 \leq \rho_{l,n}^{iiii} \leq 2$ for $i = 1, 3$
$0 \leq \rho_{l,n}^{1i1i} \leq 1/2$ for $i = 2, 3$
$-1 \leq \rho_{l,n}^{11ii} \leq 1$ for $i = 2, 3$
$\left \rho_{l,n}^{1122} \right \leq 1 - \left 1 - \rho_{l,n}^{1111} \right $
$\left \rho_{l,n}^{1133} \right \leq 1 - \left 1 - \frac{\rho_{l,n}^{1111} + \rho_{l,n}^{3333}}{2} \right $
Symmetry Constraints
$\rho_{l,n}^{1111} - 2\rho_{l,n}^{1212} - \rho_{l,n}^{1122} = 0$

Table 5: Description of decision variables, objective function, and constraints for the optimization problem in the $V_L V_L \rightarrow V_L V_L$ case. Here the $C_{r,i_r}^{ijkl}(l)$ s are polynomials in l , see [18]

We also discretize the null-constraints in a similar fashion. Thus we finally obtain expressions for the coefficients, $\tilde{c}_{ijkl}^{m,n}$, written as linear combinations of discretized spectral densities $\rho_{l,n}^{ijkl}$ which are subjected to null-constraints, unitarity constraints and constraints arising from $U(1)_{em}$ symmetry. Optimizing linear combinations of $\tilde{c}_{ijkl}^{m,n}$ over all possible variables $\rho_{l,n}^{ijkl}$ that respects a set of linear constraints, is a well-defined linear programming problem. For this work, we are only interested in the terms that are most important phenomenologically, namely, the $\tilde{c}_{ijkl}^{2,0}$. With our assumption that EFT loops can be neglected, these can be expressed as some linear combinations of WCs of HEFT operators in Table 1. In Table 5 we explicitly summarize the linear programming model that constrains $\tilde{c}_{ijkl}^{2,0}$ s related to the $V_L V_L \rightarrow V_L V_L$ scattering amplitude.

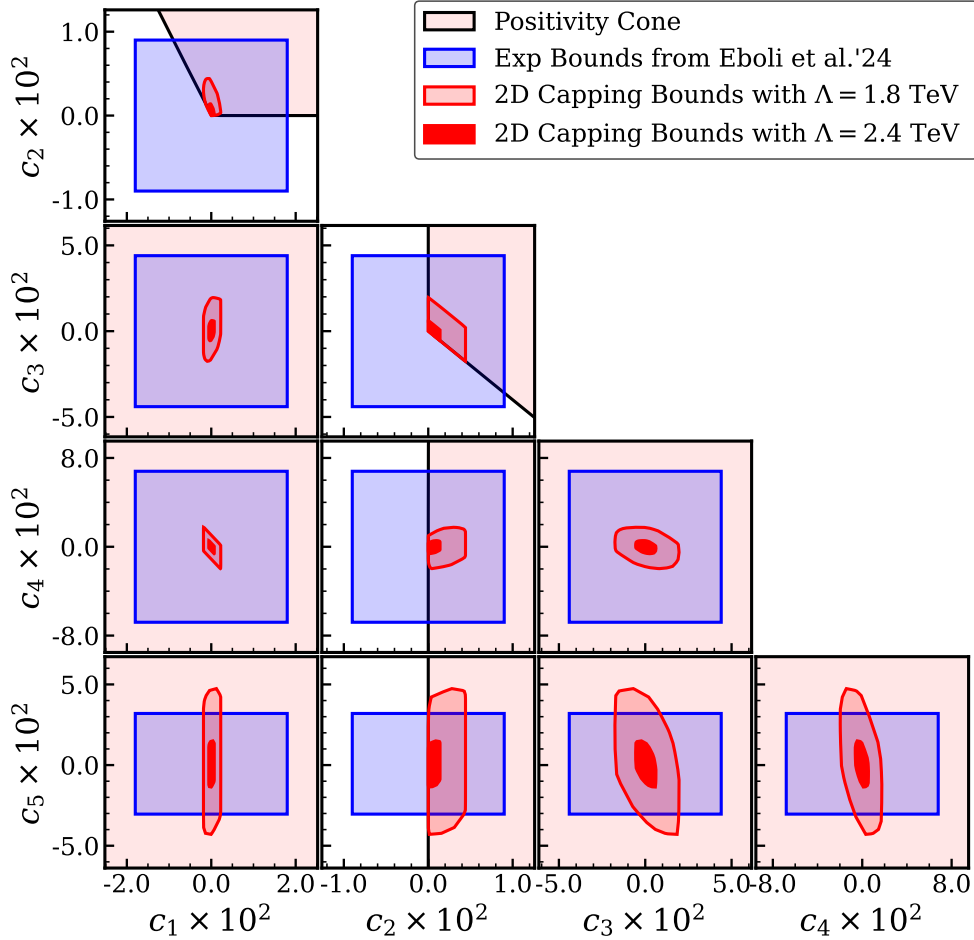


Figure 1: We show the region allowed by positivity constraints in the 5-dimensional space of the WCs, $c_1 - c_5$, contributing to the longitudinal vector boson scattering, $V_L V_L \rightarrow V_L V_L$. These constraints can be directly translated to the space of TGCs and aQGCs using the mapping provided in Table 2. In pink we show the conical region allowed by the analytical constraints in Table 4. The solid red line shows the boundary of the region allowed after the double-sided bounds are imposed using the numerical procedure detailed in Sec. 4 is followed taking, $\Lambda = 1.8$ TeV, whereas in dark red we show the region obtained by the same procedure taking, $\Lambda = 2.4$ TeV. The bounds on a particular 2-dimensional plane are obtained after marginalizing all other directions. The blue shaded region is the experimentally allowed region derived in Ref. [51].

5 Visualizing the HEFT-hedron: final positivity constraints

In this section we first present our final constraints on the HEFT WCs of Table 1 in Sec. 5.1. We then discuss the implications of applying the SMEFT constraints from Table 3 in Sec. 5.2.

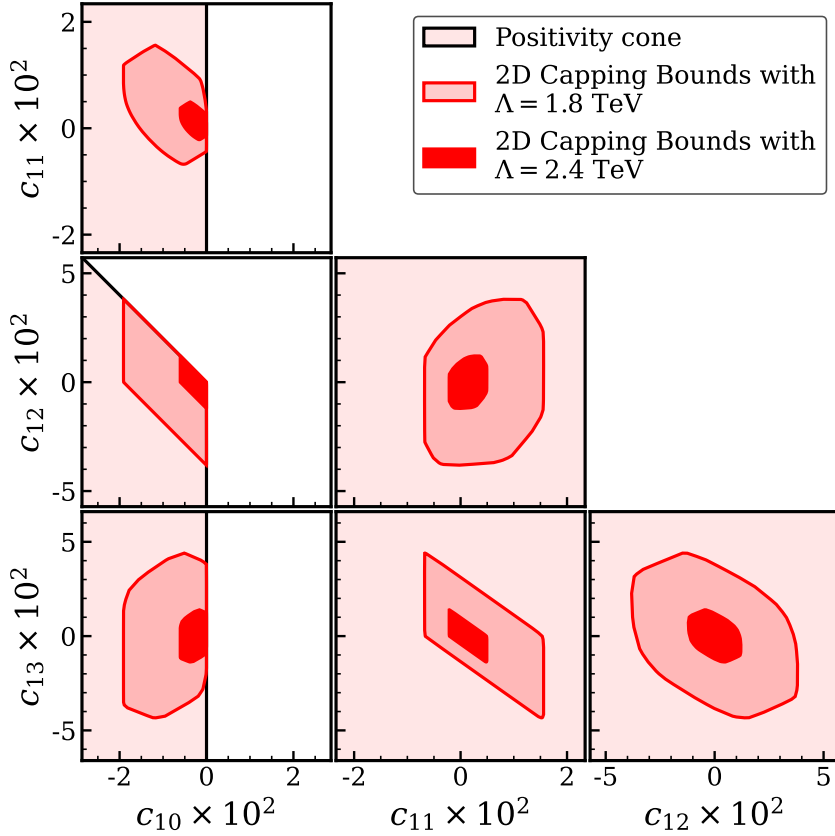


Figure 2: We show the region allowed by positivity constraints in the 5-dimensional space of the WCs, $c_{10} - c_{13}$, contributing to the scattering, $V_L V_L \rightarrow hh$. Again, the constraints can be directly translated to the space of anomalous couplings using the mapping provided in Table 2. The pink region shows the allowed conical region derived from the analytical constraints in Table 4. The solid red line shows the boundary of the allowed region derived using the numerical procedure detailed in Sec. 4 with $\Lambda = 1.8$ TeV. In dark red we show the region obtained by the same procedure but with $\Lambda = 2.4$ TeV. Once again, the bounds on a particular 2-dimensional plane are obtained after marginalizing all other directions.

5.1 Positivity constraints on HEFT WCs

In Fig. 1, 2 and 3 we, respectively, show the bounds on the WCs contributing to $V_L V_L \rightarrow V_L V_L$, $V_L V_L \rightarrow hh$ and $V_L V_L \rightarrow V_L h$ processes. For each of the three subsets of WCs we present the projection of our bounds on all possible two dimensional planes. In Table 6 we present the our final constraint on each individual WC after marginalizing over all others. Table 6 also includes bounds on c_{14} , the only operator contributing to the $V_L h \rightarrow hh$ amplitude, and c_{15} , the only operator contributing to the $hh \rightarrow hh$ process. Our bounds can be directly translated to the space of anomalous couplings using the mapping provided in Table 2.

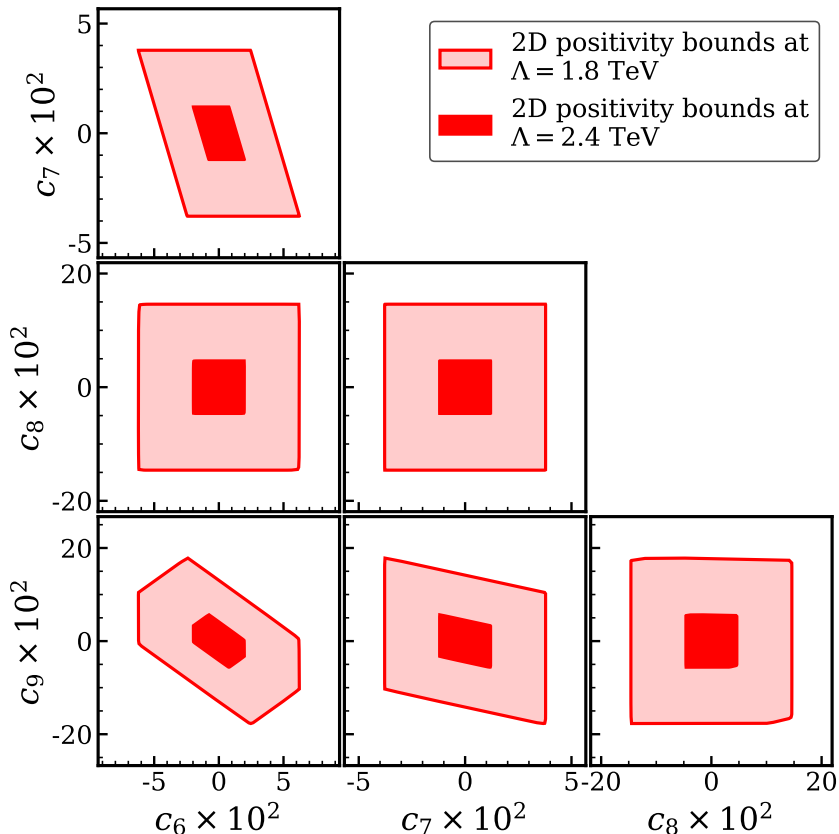


Figure 3: Bounds on the WCs $c_6 - c_8$ using the second set of positivity constraints on Table relations. For the upper bound on the right hand side of these inequalities we use the numerical capping bounds in Figs. 1 and 2 and eq. (5.2) for $\Lambda = 1.8$ TeV and 2.4 TeV. The allowed region in light and dark red, respectively, correspond to the former and latter choice of Λ .

Constraints on WCs contributing to $V_L V_L \rightarrow V_L V_L$

First, we present the bounds on the WCs contributing to longitudinal vector boson scattering, $V_L V_L \rightarrow V_L V_L$ process, i.e the set of 5 WCs, $\{c_1, c_2 \dots c_5\}$, in Fig. 1. We show the positivity constraints obtained in this work in different shades of red whereas the experimental bounds have been shown in blue. The pink region shows the region allowed after applying the analytical constraints in Table 4—in particular the first 4 constraints from Set 1 and the first inequality from Set 2. After application of these constraints from Table 4, we find a convex conical allowed region that occupies less than 26 % of 5-dimensional region allowed by the experimental bounds shown in blue. The red boundary shows the allowed region obtained after carrying out the numerical capping procedure described in Sec. 4; the lighter (deeper) shade of red within this boundary corresponds to the choice $\Lambda = 1.8$ TeV ($\Lambda = 2.4$ TeV). The shaded regions on a particular 2-dimensional plane show the

projections of the 15-dimensional HEFT-hedron on it—i.e., we marginalize over all other 13 directions while providing the bounds. It can be seen that our final bounds are significantly stronger than the experimental bounds.

As far as the blue region in Fig. 1 is concerned, it shows the allowed region after imposing the 1-dimensional experimental bounds (see Table 6) obtained after marginalizing over all other WCs. These experimental bounds have been derived in [51] using the results from vector boson scattering searches at CMS and ATLAS [52–54]. Using our power-counting scheme in eq. (2.7), the numerical values of the experimental bounds from Table 6 can be converted to lower bounds on the new physics scale that range from $\Lambda > 0.9$ TeV to 2.6 TeV (see Table 6). The values of Λ (1.8, 2.4 TeV) used to obtain the numerical capping bounds inside the red solid line have been chosen to be in the same ballpark as these experimental lower bounds.

Constraints on WCs contributing to $V_L V_L \rightarrow hh$

We now present the bounds on the WCs contributing to the, $V_L V_L \rightarrow hh$ process, i.e the set of 4 WCs, $\{c_{10}, c_{11} \cdots c_{13}\}$, in Fig. 2. Once again in pink we show the region allowed after applying the analytical constraints in Table 4 (specifically the 5th and 6th relations from the first set). The red boundary has been obtained numerically using the methods of Sec. 4 taking $\Lambda = 1.8$ TeV; the deeper shade of red within region corresponds to taking $\Lambda = 2.4$ TeV. Once again the bounds on a particular 2-dimensional plane are obtained after marginalising all other directions.

Constraints on WCs contributing to $V_L V_L \rightarrow V_L h$

In Fig. 3 we show bounds on the WCs contributing to the $V_L V_L \rightarrow V_L h$ process, namely on the set, $\{c_6, c_7 \cdots c_9\}$. Unlike the previous figures, the red boundary has not been obtained by directly applying the numerical procedure of Sec. 4 on $c_6 - c_9$. Instead we have the second set of inequalities in Table 4 (specifically the second, third, fifth, sixth and eighth relations of Set 2) to put an upper bound on $c_6 - c_9$ using upper bounds on the other WCs which appear on the right hand side of these inequalities and contribute to the processes, $V_L V_L \rightarrow V_L V_L, hh$ and $hh \rightarrow hh$ processes. For the upper bounds on the latter set of WCs, we do use the numerical bounds for $\Lambda = 1.8$ TeV and 2.4 TeV (shown in Fig. 1 and Fig. 2) that respectively result in the allowed region shown in light (dark) red in Fig. 3. In the future if experimental bounds on the WCs contributing to the $V_L V_L \rightarrow V_L V_L, hh$ processes become stronger than the capping ones, we can use them instead to bound the right hand side of the inequalities in Table 4.

Constraints on WCs contributing to $hh \rightarrow V_L h, hh$

Finally, let us provide constraints on c_{14} , which is the only WC contributing to the $VV \rightarrow Vh$ process, and c_{15} , the only WC contributing to the $hh \rightarrow hh$ process. We obtain,

$$|c_{14}| \left(\frac{\Lambda}{1.8 \text{ TeV}}\right)^4 < 0.112 \quad (5.1)$$

$$0 < c_{15} \left(\frac{\Lambda}{1.8 \text{ TeV}}\right)^4 < 0.021 \quad (5.2)$$

Process	Coefficients	Exp Bounds		Capping bounds $\times 10^2$	
		$c_i \times 10^2$	Λ (TeV)	$\Lambda = 1.8$ TeV	$\Lambda = 2.4$ TeV
$V_L V_L \rightarrow V_L V_L$	c_1	[-1.8, 1.8]	1.8	[-0.18, 0.22]	[-0.06, 0.07]
	c_2	[-0.9, 0.9]	2.6	[0, 0.44]	[0, 0.14]
	c_3	[-4.4, 4.4]	1.2	[-1.76, 1.95]	[-0.56, 0.62]
	c_4	[-6.8, 6.8]	0.9	[-1.94, 1.75]	[-0.61, 0.55]
	c_5	[-3.0, 3.2]	1.4	[-4.31, 4.78]	[-1.36, 1.51]
$V_L V_L \rightarrow V_L h$	c_6	—	—	[-6.20, 6.20]	[-1.96, 1.96]
	c_7	—	—	[-3.78, 3.78]	[-1.20, 1.20]
	c_8	—	—	[-14.60, 14.60]	[-4.62, 4.62]
	c_9	—	—	[-17.78, 17.78]	[-5.62, 5.62]
$V_L V_L \rightarrow hh$	c_{10}	—	—	[-1.91, 0]	[-0.60, 0]
	c_{11}	—	—	[-0.68, 1.56]	[-0.21, 0.49]
	c_{12}	—	—	[-3.81, 3.81]	[-1.20, 1.20]
	c_{13}	—	—	[-4.40, 4.40]	[-1.39, 1.39]
$V_L h \rightarrow hh$	c_{14}	—	—	[-11.24, 11.24]	[-3.55, 3.55]
$hh \rightarrow hh$	c_{15}	—	—	[0, 2.07]	[0, 0.66]

Table 6: Experimental and positivity bounds on the WCs of HEFT operators in Table 1. The third column presents experimental bounds on the WCs as reported in [51]. The fourth and fifth columns provide the positivity bounds which incorporate both the analytical constraints of Table 4 and the numerical capping bounds for two choices of the new physics scale (Λ): 1.8 TeV and 2.4 TeV. For both the experimental and positivity bounds, the final constraint on each individual WC has been obtained after marginalizing over all others.

where the positivity of c_{15} follows from the analytical method described in Sec. 3.3 and the upper bounds on the magnitude of c_{14} and c_{15} have been obtained following the procedure of Sec. 4.

5.2 Positivity constraints in the SMEFT

In this section we will obtain the regions in the HEFT parameter space that are consistent with both positivity constraints as well as the SMEFT at dimension-8 level, i.e. they obey the constraints of Table 6. We will consider the case of WCs contributing to $V_L V_L \rightarrow V_L V_L$ in this section and discuss similar analyses for the $V_L V_L \rightarrow hh, V_L h$ processes later in Appendix C. In Fig. 4 we show, in blue, the regions that are consistent with the SMEFT

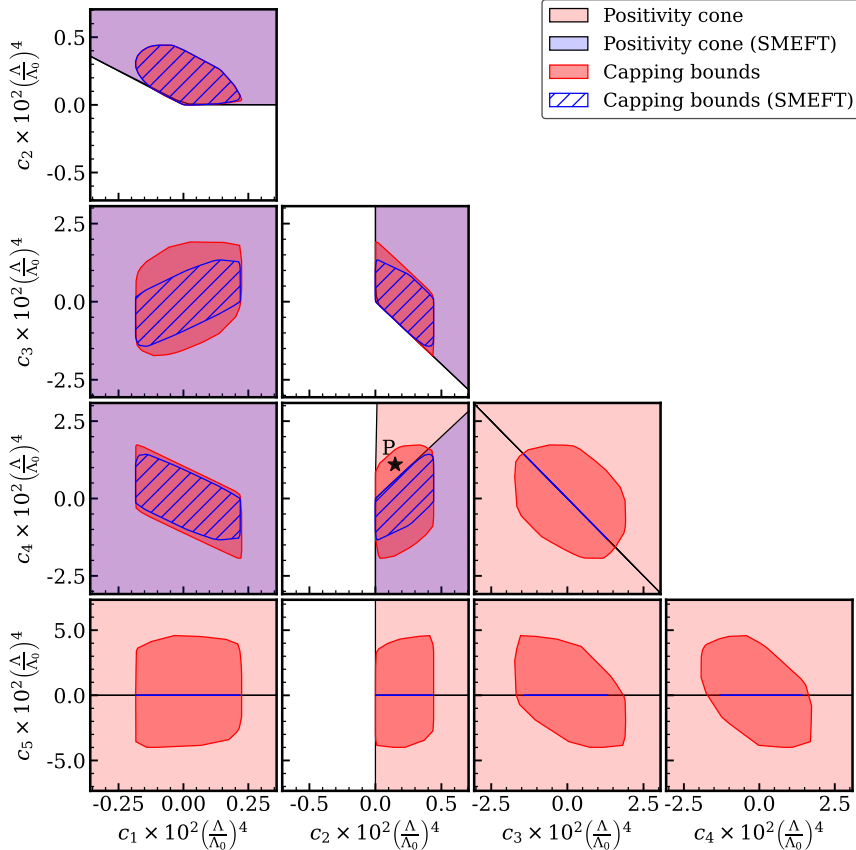


Figure 4: This figure compares the regions allowed by positivity constraints for NLO HEFT operators contributing to longitudinal vector boson scattering, $V_L V_L \rightarrow V_L V_L$, before and after imposing the requirements of the dimension-8 SMEFT (see Table 3). The pink region represents the bounds for HEFT, derived using the constraints listed in Table 4, while the darker red region shows the capping bounds for HEFT, obtained through the numerical procedure described in Sec. 4. The light blue region (the blue hatched region) represents the regions consistent with the analytical positivity (numerical capping) bounds as well as the SMEFT requirements of Table 3. The point, P , represents a measurement that lies outside the light blue allowed region in SMEFT but within the pink region consistent with the HEFT positivity cone. Here, we have taken, $\Lambda_0 = 1.8$ TeV.

constraints in Table 3 as well as the analytical positivity constraints of Table 4. The blue hatched region in Fig. 4 represents the region consistent with both the SMEFT constraints and the numerical capping bounds.⁹ Geometrically these regions represent the projection of—the intersection of the the 15 dimensional region allowed by positivity constraints with the 3 dimensional SMEFT hyperplane—on the different 2-dimensional HEFT planes in

⁹Note that as far as the numerical capping bounds are concerned, we expect them to be less stringent than the bounds obtained in Ref. [18, 49]. This is because Ref. [18, 49] used the full $SU(2)_L \times U(1)_Y$ symmetry to constrain the spectral densities to obtain the double-sided bounds (see Sec. 4). Our assumption, that the spectral densities satisfy $U(1)_{em}$ invariance, is thus less restrictive than that of Ref. [18, 49].

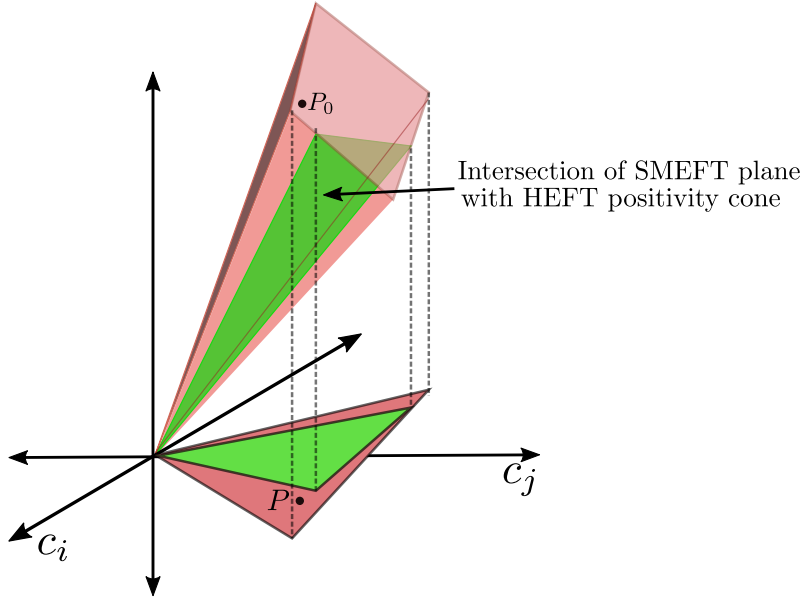


Figure 5: A schematic diagram showing HEFT positivity cone (pink) and its intersection with SMEFT plane (green) and the projection of these two regions on the space of the 2 HEFT WCs c_i and c_j .

Fig. 4. For the case of the analytical positivity constraints, we show this schematically in Fig. 5. Recall that the SMEFT positivity cone, i.e the intersection of the SMEFT plane and the HEFT positivity cone, was derived in eq. (3.8).

The regions in Fig. 4 in pink (red) represent the region allowed in the HEFT by analytical (numerical) positivity bounds. They represent the projection of the full 15-dimensional allowed region—and not just the intersection with the SMEFT plane—on the various 2-dimensional planes of Fig. 4. As shown in Fig. 5, we expect them to be generally larger than the corresponding blue (hatched blue) region consistent with SMEFT. This fact has important implications that were recently pointed out in Ref. [26]. Consider, for instance, the scenario where HEFT is the correct EFT to describe nature and a non-zero measurement, P , is made in the $c_2 - c_4$ plane such that is outside the region consistent with the SMEFT positivity cone, but within the region consistent with the HEFT positivity cone (see Fig. 4). If one wrongly assumes that SMEFT is the correct EFT at low-energies, such a measurement would not necessarily be indicative of the breakdown of unitarity or causality but might only mean that the correct low energy EFT is not the SMEFT, but a more general HEFT. ¹⁰

As shown in Fig. 5, this possibility can arise only if the correct theory of nature corresponds to a point, P_0 , in the 15-dimensional HEFT space that lies outside the SMEFT

¹⁰Note that if P was only outside the region allowed by capping but not outside the region consistent with the positivity cone, it would be more difficult to draw any of these inferences. This is because with the choice of a smaller, Λ , the region allowed by the capping bounds would become larger and might start including the point, P . Strong conclusions can be drawn in this case only if experiments definitively exclude any possibility of new physics below the chosen cutoff scale, Λ .

plane. Its projection, P , on the $c_2 - c_4$ plane would then lie outside the blue region. This would still not be very surprising if all the HEFT WCs, $c_1 - c_{15}$ can be independently measured—recall that there is a one-to-one mapping between these HEFT WCs and the the forward amplitude for different channels of longitudinal gauge-Higgs scattering (see eq. (2.43)). This is because one could then directly check that the SMEFT constraints in Table 3 are violated—that is the theory lies outside the SMEFT plane. For such a scenario, the positivity conditions of Table 4 would add no new information over what is already contained in Table 3.

In practice, however, not all of the HEFT WCs, $c_1 - c_{15}$, would be measurable. The observation made in Ref. [26] can then become truly powerful. Consider, for instance, the hypothetical scenario where future experiments are sensitive only to the HEFT WCs c_2 and c_4 . As all values of c_2 and c_4 are consistent with requirements of Table 3, there would be no way to use these requirements to infer that SMEFT is the wrong low-energy description. Measurements converging at the point P outside the SMEFT positivity region might then provide the first indication that SMEFT is not the correct EFT description.

Finally, let us discuss another subtlety that may arise if one wishes to utilize the proposal of Ref. [26]. Ref. [26] demonstrated that taking only the 5 custodial invariant operators of Table 1, the projection of the HEFT positivity cone on the SMEFT plane is larger than than their intersection region. When one projects to a certain set of observables, however, this feature may be lost. For instance, let us consider the possibility of utilizing the proposal of Ref. [26] in vector boson scattering measurements. We must then project to the plane of the only custodial invariant operators contributing to this process, namely the $c_1 - c_2$ plane. We see in Fig. 4 that the regions allowed by SMEFT and HEFT positivity constraints in this plane are, unfortunately, identical. One can, in fact, explicitly check that if the value of SMEFT WCs is fixed by a measurement of only c_1 and c_2 , and if these two WCs satisfy the HEFT positivity constraints in Table 4, the inferred SMEFT WCs will always be in the SMEFT positivity cone defined by eq. (3.8). Thus in the custodial limit, there is no way to distinguish SMEFT from HEFT using aQGC measurements alone. If we consider the $V_L V_L \rightarrow hh$ process, however, the relevant plane of custodial invariant operators is the $c_{10} - c_{11}$ plane and the region allowed in HEFT is then clearly larger than that in SMEFT, see Fig. 6.

We discuss in the implications of the SMEFT constraints of Table 3 on the $V_L V_L \rightarrow V_L V_L, V_L h$ process in Appendix C.

6 Conclusions

We derive the consequences of causality/analyticity and unitarity on the classic problem of scattering among longitudinal electroweak and Higgs bosons. In particular, we derive the constraints from these theoretical requirements on the the coefficient of s^2 in the forward amplitude for these processes. Using only $U(1)_{em}$ invariance, we show that the s^2 piece of the forward amplitudes of longitudinal gauge-Higgs scattering processes can be parameterized by 15 independent parameters (see Sec. 2.4). We also provide a one-to one mapping of these 15 parameters with 15 WCs of the NLO HEFT lagrangian (see eq. (2.43)) and

15 independent linear combinations of anomalous couplings of a $U(1)_{em}$ lagrangian (see Table 2). As far as the HEFT is concerned, no other scattering process grows as s^2 or faster at NLO, so that considering only these 15 operators allows us to obtain the complete set of bounds at NLO. In the SMEFT only three operators contribute to the s^2 piece of the forward amplitudes up to dimension-8 level. Thus the SMEFT truncated at dimension-8 level implies 12 constraints on the space of HEFT WCs, that we present in Table 3.

We then derive analytical positivity constraints on the space of these 15 HEFT WCs. These have been presented in Table 4 in two sets. The first set of constraints requires the positivity of some linear combinations of CP-even WCs contributing to the elastic processes, $V_L h \rightarrow V_L h$, $Z_L Z_L \rightarrow Z_L Z_L$, $W_L W_L \rightarrow W_L W_L$, $W_L Z_L \rightarrow W_L Z_L$ and $hh \rightarrow hh$. The second set of constraints, imply that the magnitude of certain WCs—including all CP-odd ones—that contribute to the inelastic processes, $V_L V_L \rightarrow h V_L$, $hh \rightarrow V_L h$, must be smaller than products of the WCs constrained by the first set. A non-vanishing WC contributing to the $V_L V_L \rightarrow h V_L$, $hh \rightarrow V_L h$ processes, would thus imply that some of the other WCs contributing to the elastic processes must be non-zero. Together these analytical constraints define a positivity cone within which the HEFT WCs must lie. They rule out about 95 % of the full 15-dimensional HEFT space and about about 74 % of the 5 dimensional space still allowed by experimental bounds from vector boson scattering processes.

We then go on to derive numerical double-sided bounds on the HEFT WCs, that cap this positivity cone. Our final results, shown in Fig. 1-3 and Table 6, provide the first reported bound on the WCs contributing to the $V_L V_L \rightarrow V_L h$, hh and $hh \rightarrow V_L h$, hh processes. For the case of vector boson scattering, they significantly improve over existing experimental bounds. Finally, we obtain the region in HEFT space allowed by positivity as well as the requirements of the dimension-8 SMEFT. We then comment on the possibility [26] of using positivity bounds to infer that the HEFT—and not the SMEFT—is the correct low energy EFT.

The LHC has only begun to probe the scattering of gauge and Higgs bosons—a set of processes of great conceptual importance. With the large increase in integrated luminosity expected in the coming decades, it will be able to probe the 15-dimensional space of EFT WCs discussed here with greater and greater precision. Our results provide theoretical priors on this space to complement this important experimental program.

Acknowledgements

We are grateful to Amol Dighe for insightful discussions and suggestions on how to visually present our multidimensional bounds. We also thank Avik Banerjee, Shankha Banerjee and Siddhartha Karmakar for useful discussions. We acknowledge the support from the Department of Atomic Energy (DAE), Government of India, under Project Identification Number RTI 4002.

A Vector boson scattering in the unitary gauge

In this section, we explicitly show that the operators in eq. (2.11) (eq. (2.26)) in the HEFT (SMEFT) do not give rise to s^2 growth in the vector boson scattering amplitude. The s^2 piece in the scattering amplitudes of longitudinal gauge bosons W_L^\pm, Z_L , contains not only contributions from the aQGCs but also from the TGCs as noted in the main text (see Section 2.2). When we take into account all the TGCs and aQGCs generated by eq. (2.11) and eq. (2.26), however, their contributions to the s^2 term cancels out.

First of all, for the process $Z_L Z_L \rightarrow Z_L Z_L$, the only anomalous coupling that contributes is the aQGC, h_{ZZ}^Q ; this aQGC receives no contribution from the operators in eq. (2.11) (eq. (2.26)) in the HEFT (SMEFT). For the other processes the amplitude is given by,

$$\begin{aligned}
\mathcal{M}_{W+W^- \rightarrow W+W^-}(s, t) &= - \left(\frac{g^2 c_{\theta_W}^2}{2M_W^4} \delta\kappa_Z + \frac{g^2 s_{\theta_W}^2}{2M_W^4} \delta\kappa_\gamma \right) (s^2 + 4st + t^2) \\
&\quad + \frac{g^2}{4M_W^4} \left(2\delta g_{WW1}^Q (s+t)^2 - \delta g_{WW2}^Q (s^2 + t^2) \right) \\
\mathcal{M}_{W+Z \rightarrow W+Z}(s, t) &= - \frac{g^2 c_{\theta_W}^2}{4m_W^2 m_Z^2} \left(2\delta g_1^Z (2s^2 + 2st - t^2) - \delta g_{ZZ1}^Q (2s^2 + 2st + t^2) \right. \\
&\quad \left. + 2\delta g_{ZZ2}^Q t^2 \right). \tag{A.1}
\end{aligned}$$

Here we have retained only the terms which grow quadratically with energy. All other amplitudes involving four longitudinal gauge bosons can be derived from the above two amplitudes via crossing symmetry relations. We can explicitly check from eq. (2.12-2.15) in the HEFT, and eq. (2.31-2.32) in the SMEFT that the amplitude in eq. (A.1) has no dependence on the WCs of the operators in question.

B Derivation of Positivity Constraints on HEFT Operators at NLO

In this section, we provide a detailed discussion of how we derived the positivity constraints presented in Table 4. As outlined in eq. (3.7), we exploit the fact that the matrix γ_β , defined as

$$(\gamma_\beta)_{ik} = \beta_j \beta_l^* \frac{\partial^2}{\partial s^2} \tilde{\mathcal{M}}_{ijkl}(s, t \rightarrow 0)|_{s=0}, \tag{B.1}$$

is positive-definite for any arbitrary choice of β , provided that the norm $\sum_{i=1}^4 |\beta_i|^2 = 1$. In this expression, the indices i, j, k , and l in $\tilde{\mathcal{M}}_{ijkl}$ take values from 1 to 4, where 1, 2, and 3 correspond to the three Goldstone bosons arising from electroweak symmetry breaking, while 4 denotes the physical Higgs field h . We can express each element of the 4×4 matrix γ_β as some linear combination of WCs of HEFT NLO operators listed in Table 1 and β

which we provide below,

$$(\gamma_{\beta})_{11} = a_1 |\beta_1|^2 + a_4 |\beta_2|^2 + a_6 |\beta_3|^2 + a_{11} |\beta_4|^2 + 2a_9 \operatorname{Re}\{\beta_3 \overline{\beta_4}\} \quad (\text{B.2})$$

$$(\gamma_{\beta})_{22} = a_4 |\beta_1|^2 + a_1 |\beta_2|^2 + a_6 |\beta_3|^2 + a_{11} |\beta_4|^2 + 2a_9 \operatorname{Re}\{\beta_3 \overline{\beta_4}\} \quad (\text{B.3})$$

$$(\gamma_{\beta})_{33} = a_6 \left(|\beta_1|^2 + |\beta_2|^2 \right) + a_5 |\beta_3|^2 + a_{13} |\beta_4|^2 + 2a_{12} \operatorname{Re}\{\beta_3 \overline{\beta_4}\} \quad (\text{B.4})$$

$$(\gamma_{\beta})_{44} = a_{11} \left(|\beta_1|^2 + |\beta_2|^2 \right) + a_{13} |\beta_3|^2 + a_{16} |\beta_4|^2 + 2a_{15} \operatorname{Re}\{\beta_3 \overline{\beta_4}\} \quad (\text{B.5})$$

$$(\gamma_{\beta})_{12} = 2a_2 \operatorname{Re}\{\beta_1 \overline{\beta_2}\} \quad (\text{B.6})$$

$$(\gamma_{\beta})_{13} = 2a_3 \operatorname{Re}\{\beta_1 \overline{\beta_3}\} + 2a_7 \operatorname{Re}\{\beta_1 \overline{\beta_4}\} + 2a_{10} \operatorname{Re}\{\beta_2 \overline{\beta_4}\} \quad (\text{B.7})$$

$$(\gamma_{\beta})_{14} = 2a_7 \operatorname{Re}\{\beta_1 \overline{\beta_3}\} + 2a_8 \operatorname{Re}\{\beta_1 \overline{\beta_4}\} - 2a_{10} \operatorname{Re}\{\beta_2 \overline{\beta_3}\} \quad (\text{B.8})$$

$$(\gamma_{\beta})_{23} = -2a_{10} \operatorname{Re}\{\beta_1 \overline{\beta_4}\} + 2a_3 \operatorname{Re}\{\beta_2 \overline{\beta_3}\} + 2a_7 \operatorname{Re}\{\beta_2 \overline{\beta_4}\} \quad (\text{B.9})$$

$$(\gamma_{\beta})_{24} = 2a_{10} \operatorname{Re}\{\beta_1 \overline{\beta_3}\} + 2a_7 \operatorname{Re}\{\beta_2 \overline{\beta_3}\} + 2a_8 \operatorname{Re}\{\beta_2 \overline{\beta_4}\} \quad (\text{B.10})$$

$$(\gamma_{\beta})_{34} = a_9 \left(|\beta_1|^2 + |\beta_2|^2 \right) + a_{12} |\beta_3|^2 + a_{15} |\beta_4|^2 + 2a_{14} \operatorname{Re}\{\beta_3 \overline{\beta_4}\} \quad (\text{B.11})$$

Given that, the matrix γ_{β} is hermitian, we can express the remaining elements in terms of those already provided above. Coefficients a_i 's in Eq.(B.2-B.11) are related to the WCs c_i 's in Eq. (2.6) in the following manner,

$$\begin{aligned} a_1 &= 16(c_1 + c_2), & a_2 &= 4(2c_1 + c_2), & a_3 &= 8c_1 + 2c_2 + c_3 + 4c_4, \\ a_4 &= 8c_2, & a_5 &= 16(c_1 + c_2) + 8(c_3 + c_4) + 4c_5, & a_6 &= 2(4c_2 + c_3), \\ a_7 &= c_6 + \frac{c_7}{2}, & a_8 &= 2c_{11}, & a_9 &= c_7, & a_{10} &= -\frac{c_8}{4}, & a_{11} &= -2c_{10}, \\ a_{12} &= 2(c_6 + c_7 + c_9/2), & a_{13} &= -(2c_{10} + c_{12}), & a_{14} &= (2c_{11} + c_{13}), \\ a_{15} &= -c_{14}/2, & a_{16} &= 4c_{15}. \end{aligned} \quad (\text{B.12})$$

We intend to derive conditions on a_i s so that matrix γ_{β} satisfies positive definiteness condition for an arbitrary choice of β . To this end, we utilize the property that any principle sub-matrix of a positive definite matrix is also positive definite. First, we demand all 1×1 principle sub-matrices, i.e. the diagonal elements of γ_{β} , are positive. For example, for different choices for β , $(\gamma_{\beta})_{11} > 0$ implies,

$$a_1 > 0 \quad \beta_1 \neq 0 \text{ and } \beta_i = 0 \text{ for } i = 2, 3, 4 \quad (\text{B.13})$$

$$a_4 > 0 \quad \beta_2 \neq 0 \text{ and } \beta_i = 0 \text{ for } i = 1, 3, 4 \quad (\text{B.14})$$

$$a_6 > 0 \quad \beta_3 \neq 0 \text{ and } \beta_i = 0 \text{ for } i = 1, 2, 4 \quad (\text{B.15})$$

$$a_{11} > 0 \quad \beta_4 \neq 0 \text{ and } \beta_i = 0 \text{ for } i = 1, 2, 3 \quad (\text{B.16})$$

$$a_9^2 < a_6 a_{11} \quad \arg \beta_3 = \pi + \arg \beta_4, \quad |\beta_3|/|\beta_4| = \sqrt{a_{11}/a_6} \text{ and } \beta_{1,2} = 0. \quad (\text{B.17})$$

Following similar steps for rest of the diagonal elements of γ_{β} , we get the following set of constraints,

$$a_1, a_4, a_6, a_{11}, a_5, a_{13}, a_{16} > 0, \quad (\text{B.18})$$

$$a_9^2 < a_6 a_{11}, \quad a_{12}^2 < a_5 a_{13}, \quad a_{15}^2 < a_{13} a_{16}. \quad (\text{B.19})$$

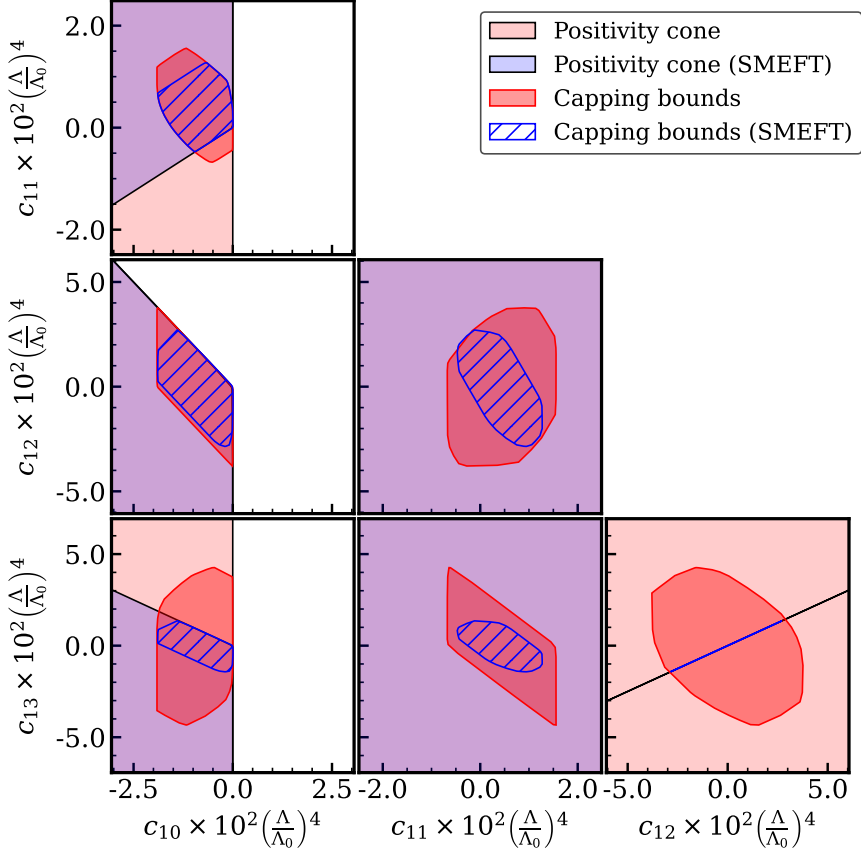


Figure 6: This figure compares the regions allowed by positivity constraints for NLO HEFT operators contributing to longitudinal vector boson scattering, $V_L V_L \rightarrow hh$, before and after imposing the requirements of the dimension-8 SMEFT (see Table 3). The pink region represents the bounds for HEFT, derived using the constraints listed in Table 4, while the darker red region shows the capping bounds for HEFT, obtained through the numerical procedure described in Sec. 4. The light blue region (the blue hatched region) represents the regions consistent with the analytical positivity (numerical capping) bounds as well as the SMEFT requirements of Table 3. Here, we have taken, $\Lambda_0 = 1.8$ TeV.

Next we consider all possible 2×2 principle sub-matrices of γ_β and derive the conditions on a_i s so that these sub-matrices remain positive definite irrespective of β . We show explicitly the process for one of the sub-matrices. Consider the following sub-matrix obtained from γ_β by deleting the second and fourth columns and rows,

$$\begin{bmatrix} (\gamma_\beta)_{11} & (\gamma_\beta)_{13} \\ (\gamma_\beta)_{31} & (\gamma_\beta)_{33} \end{bmatrix} \succ 0 \quad (\text{B.20})$$

We get following constraints from positive-definiteness of this matrix by marginalizing over

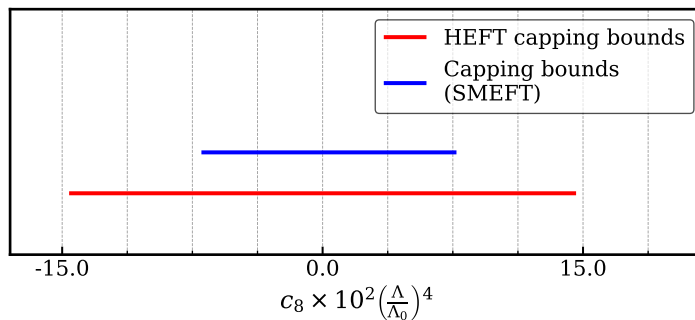


Figure 7: This figure compares the capping bounds on the WC c_8 with and without application of the SMEFT constraints. After imposing the SMEFT constraints listed in Table 3, c_8 remains the only non-vanishing WC contributing to the $V_L V_L \rightarrow V_L h$ process. The blue line represents the capping bound on c_8 with SMEFT constraints, while the red line shows the bound without them. The reference scale is set to $\Lambda_0 = 1.8 \text{ TeV}$.

β ,

$$\begin{aligned}
4a_3^2 &< (a_6 + \sqrt{a_1 a_5})^2 & \beta_1/\beta_3 &= (a_5/a_1)^{1/4} \text{ and } \beta_{2,4} = 0 \\
4a_7^2 &< (\sqrt{a_6 a_{11}} + \sqrt{a_1 a_{13}})^2 & \beta_1/\beta_4 &= (\sqrt{a_{11} a_{13}}/\sqrt{a_1 a_6})^{1/2} \text{ and } \beta_{2,3} = 0 \\
4a_{10}^2 &< (\sqrt{a_6 a_{11}} + \sqrt{a_4 a_{13}})^2 & \beta_2/\beta_4 &= (\sqrt{a_{11} a_{13}}/\sqrt{a_4 a_6})^{1/2} \text{ and } \beta_{1,3} = 0.
\end{aligned} \tag{B.21}$$

C Implications of SMEFT constraints on the $V_L V_L \rightarrow V_L V_L, hh$ process

In this appendix we present in Fig. 6 (Fig. 7) the regions in Fig. 2 (Fig. 3) consistent with the requirements of the dimension-8 SMEFT in Table 4. In Fig. 6 we again see that the region allowed by positivity is larger in the HEFT than in the SMEFT for many of the cases. This includes the $c_{10} - c_{11}$ plane of the two custodial invariant operators.

As far as the WCs contributing to, $V_L V_L \rightarrow V_L h$, are concerned only one of them, c_8 , is allowed to be non-zero in the dimension-8 SMEFT (see Table 4). We show in Fig. 7 that its allowed range shrinks significantly once we impose the SMEFT restrictions of Table 4.

References

- [1] ATLAS collaboration, *Observation of a new particle in the search for the Standard Model Higgs boson with the ATLAS detector at the LHC*, *Phys. Lett. B* **716** (2012) 1 [[1207.7214](#)].
- [2] CMS collaboration, *Observation of a New Boson at a Mass of 125 GeV with the CMS Experiment at the LHC*, *Phys. Lett. B* **716** (2012) 30 [[1207.7235](#)].
- [3] A. Adams, N. Arkani-Hamed, S. Dubovsky, A. Nicolis and R. Rattazzi, *Causality, analyticity and an ir obstruction to uv completion*, *Journal of High Energy Physics* **2006** (2006) 014.
- [4] T.N. Pham and T.N. Truong, *Evaluation of the derivative quartic terms of the meson chiral lagrangian from forward dispersion relations*, *Phys. Rev. D* **31** (1985) 3027.

- [5] B. Ananthanarayan, D. Toublan and G. Wanders, *Consistency of the chiral pion pion scattering amplitudes with axiomatic constraints*, *Phys. Rev. D* **51** (1995) 1093 [[hep-ph/9410302](#)].
- [6] M.R. Pennington and J. Portoles, *The Chiral Lagrangian parameters, l_1 , l_2 , are determined by the rho resonance*, *Phys. Lett. B* **344** (1995) 399 [[hep-ph/9409426](#)].
- [7] B. Bellazzini, J. Elias Miró, R. Rattazzi, M. Riembau and F. Riva, *Positive moments for scattering amplitudes*, *Phys. Rev. D* **104** (2021) 036006 [[2011.00037](#)].
- [8] A.J. Tolley, Z.-Y. Wang and S.-Y. Zhou, *New positivity bounds from full crossing symmetry*, *JHEP* **05** (2021) 255 [[2011.02400](#)].
- [9] S. Caron-Huot and V. Van Duong, *Extremal Effective Field Theories*, *JHEP* **05** (2021) 280 [[2011.02957](#)].
- [10] N. Arkani-Hamed, T.-C. Huang and Y.-t. Huang, *The EFT-Hedron*, *JHEP* **05** (2021) 259 [[2012.15849](#)].
- [11] A. Sinha and A. Zahed, *Crossing Symmetric Dispersion Relations in Quantum Field Theories*, *Phys. Rev. Lett.* **126** (2021) 181601 [[2012.04877](#)].
- [12] B. Bellazzini and F. Riva, *New phenomenological and theoretical perspective on anomalous ZZ and $Z\gamma$ processes*, *Phys. Rev. D* **98** (2018) 095021 [[1806.09640](#)].
- [13] C. Zhang and S.-Y. Zhou, *Positivity bounds on vector boson scattering at the LHC*, *Phys. Rev. D* **100** (2019) 095003 [[1808.00010](#)].
- [14] Q. Bi, C. Zhang and S.-Y. Zhou, *Positivity constraints on aQGC: carving out the physical parameter space*, *JHEP* **06** (2019) 137 [[1902.08977](#)].
- [15] G.N. Remmen and N.L. Rodd, *Consistency of the Standard Model Effective Field Theory*, *JHEP* **12** (2019) 032 [[1908.09845](#)].
- [16] G.N. Remmen and N.L. Rodd, *Flavor Constraints from Unitarity and Analyticity*, *Phys. Rev. Lett.* **125** (2020) 081601 [[2004.02885](#)].
- [17] D. Ghosh, R. Sharma and F. Ullah, *Amplitude’s positivity vs. subluminality: causality and unitarity constraints on dimension 6 & 8 gluonic operators in the SMEFT*, *JHEP* **02** (2023) 199 [[2211.01322](#)].
- [18] Q. Chen, K. Mimasu, T.A. Wu, G.-D. Zhang and S.-Y. Zhou, *Capping the positivity cone: dimension-8 Higgs operators in the SMEFT*, [2309.15922](#).
- [19] A. Falkowski and R. Rattazzi, *Which EFT*, *JHEP* **10** (2019) 255 [[1902.05936](#)].
- [20] T. Cohen, N. Craig, X. Lu and D. Sutherland, *Is SMEFT Enough?*, *JHEP* **03** (2021) 237 [[2008.08597](#)].
- [21] I. Banta, T. Cohen, N. Craig, X. Lu and D. Sutherland, *Non-decoupling new particles*, *JHEP* **02** (2022) 029 [[2110.02967](#)].
- [22] C. Zhang and S.-Y. Zhou, *Convex Geometry Perspective on the (Standard Model) Effective Field Theory Space*, *Phys. Rev. Lett.* **125** (2020) 201601 [[2005.03047](#)].
- [23] J. Distler, B. Grinstein, R.A. Porto and I.Z. Rothstein, *Falsifying models of new physics via ww scattering*, *Phys. Rev. Lett.* **98** (2007) 041601.
- [24] L. Vecchi, *Causal vs. analytic constraints on anomalous quartic gauge couplings*, *Journal of High Energy Physics* **2007** (2007) 054.

- [25] D. Chakraborty, S. Chattopadhyay and R.S. Gupta, *Towards the HEFT-hedron: the complete set of positivity constraints on HEFT operators at NLO. Presented at the 8th General Meeting of the LHC EFT Working Group*, December, 2024, [Link to talk](#).
- [26] G.N. Remmen and N.L. Rodd, *Positively Identifying HEFT or SMEFT*, [2412.07827](#).
- [27] A.C. Longhitano, *Heavy Higgs Bosons in the Weinberg-Salam Model*, *Phys. Rev. D* **22** (1980) 1166.
- [28] A.C. Longhitano, *Low-Energy Impact of a Heavy Higgs Boson Sector*, *Nucl. Phys. B* **188** (1981) 118.
- [29] T. Appelquist and C. Bernard, *Strongly interacting higgs bosons*, *Phys. Rev. D* **22** (1980) 200.
- [30] T. Appelquist and G.-H. Wu, *The Electroweak chiral Lagrangian and new precision measurements*, *Phys. Rev. D* **48** (1993) 3235 [[hep-ph/9304240](#)].
- [31] G. Buchalla and O. Cata, *Effective Theory of a Dynamically Broken Electroweak Standard Model at NLO*, *JHEP* **07** (2012) 101 [[1203.6510](#)].
- [32] R. Alonso, M.B. Gavela, L. Merlo, S. Rigolin and J. Yepes, *The Effective Chiral Lagrangian for a Light Dynamical "Higgs Particle"*, *Phys. Lett. B* **722** (2013) 330 [[1212.3305](#)].
- [33] G. Buchalla, O. Catà and C. Krause, *Complete Electroweak Chiral Lagrangian with a Light Higgs at NLO*, *Nucl. Phys. B* **880** (2014) 552 [[1307.5017](#)].
- [34] I. Brivio, T. Corbett, O.J.P. Éboli, M.B. Gavela, J. Gonzalez-Fraile, M.C. Gonzalez-Garcia et al., *Disentangling a dynamical Higgs*, *JHEP* **03** (2014) 024 [[1311.1823](#)].
- [35] I. Brivio, J. Gonzalez-Fraile, M.C. Gonzalez-Garcia and L. Merlo, *The complete HEFT Lagrangian after the LHC Run I*, *Eur. Phys. J. C* **76** (2016) 416 [[1604.06801](#)].
- [36] H. Sun, M.-L. Xiao and J.-H. Yu, *Complete nlo operators in the higgs effective field theory*, *Journal of High Energy Physics* **2023** (2023) 43.
- [37] M.S. Chanowitz, M. Golden and H. Georgi, *Low-Energy Theorems for Strongly Interacting W's and Z's*, *Phys. Rev. D* **36** (1987) 1490.
- [38] L. Gráf, B. Henning, X. Lu, T. Melia and H. Murayama, *Hilbert series, the Higgs mechanism, and HEFT*, *JHEP* **02** (2023) 064 [[2211.06275](#)].
- [39] J.M. Cornwall, D.N. Levin and G. Tiktopoulos, *Derivation of gauge invariance from high-energy unitarity bounds on the s matrix*, *Phys. Rev. D* **10** (1974) 1145.
- [40] K. Hagiwara, R.D. Peccei, D. Zeppenfeld and K. Hikasa, *Probing the Weak Boson Sector in $e^+ e^- \rightarrow W^+ W^-$* , *Nucl. Phys. B* **282** (1987) 253.
- [41] J. Reuter, W. Kilian and M. Sekulla, *Simplified Models for New Physics in Vector Boson Scattering - Input for Snowmass 2013*, [1307.8170](#).
- [42] B. Henning, X. Lu, T. Melia and H. Murayama, *2, 84, 30, 993, 560, 15456, 11962, 261485, ...: Higher dimension operators in the SM EFT*, *JHEP* **08** (2017) 016 [[1512.03433](#)].
- [43] H.-L. Li, Z. Ren, J. Shu, M.-L. Xiao, J.-H. Yu and Y.-H. Zheng, *Complete set of dimension-eight operators in the standard model effective field theory*, *Phys. Rev. D* **104** (2021) 015026 [[2005.00008](#)].
- [44] B. Bellazzini, M. Riembau and F. Riva, *IR side of positivity bounds*, *Phys. Rev. D* **106** (2022) 105008 [[2112.12561](#)].

- [45] M. Chala and J. Santiago, *Positivity bounds in the standard model effective field theory beyond tree level*, *Phys. Rev. D* **105** (2022) L111901 [2110.01624].
- [46] M. Froissart, *Asymptotic behavior and subtractions in the Mandelstam representation*, *Phys. Rev.* **123** (1961) 1053.
- [47] A. Martin, *Extension of the axiomatic analyticity domain of scattering amplitudes by unitarity. 1.*, *Nuovo Cim. A* **42** (1965) 930.
- [48] C. de Rham, S. Melville, A.J. Tolley and S.-Y. Zhou, *Positivity bounds for scalar field theories*, *Phys. Rev. D* **96** (2017) 081702 [1702.06134].
- [49] D.-Y. Hong, Z.-H. Wang and S.-Y. Zhou, *On Capped Higgs Positivity Cone*, 4, 2024 [2404.04479].
- [50] P. Virtanen, R. Gommers, T.E. Oliphant, M. Haberland, T. Reddy, D. Cournapeau et al., *SciPy.optimize.linprog*. SciPy Developers, 2020.
- [51] O.J.P. Eboli, M.C. Gonzalez-Garcia and M. Martinez, *Bounds on Quartic Gauge Couplings in HEFT from Electroweak Gauge Boson Pair Production at the LHC*, 2311.09300.
- [52] A.S. et al. (CMS), *Evidence for electroweak production of four charged leptons and two jets in proton-proton collisions at $s=13\text{TeV}$* , *Physics Letters B* **812** (2021) 135992.
- [53] A.S. et al. (CMS), *Measurements of production cross sections of wz and same-sign ww boson pairs in association with two jets in proton-proton collisions at $s=13\text{TeV}$* , *Physics Letters B* **809** (2020) 135710.
- [54] T.A. Aad, G. et al. collaboration, *Differential cross-section measurements of the production of four charged leptons in association with two jets using the atlas detector*, *Journal of High Energy Physics* **2024** (2024) 4.